Stokes flow past a compound drop in a circular tube

Yanxi Song, Jinliang Xu,[a] and Yongping Yang
Beijing Key Laboratory of New and Renewable Energy, North China Electric Power University, Beijing 102206, People's Republic of China

(Received 20 November 2009; accepted 7 June 2010; published online 22 July 2010)

Microfluidics could generate drops or bubbles with controllable size and frequency at this stage. However, analytical work on such problem is less reported in the literature. In this study, we study the motion of a compound drop, consisting of a fluid drop engulfed in a larger drop, confined in a circular tube. The analysis is based on the low Reynolds number Stokes flow theory. Interfaces are assumed to be spherical due to large surface tension. Stream functions in one bipolar and two cylindrical coordinate systems are developed in series form. Our new contribution is the transformation between cylindrical and bipolar coordinate systems. Flow patterns are mainly dependent on the relative motion and the size of the inner drop. Four types of flow patterns are identified. Drag force on the inner or outer drops is in proportion to the product of the drop radius and viscosity of the phase encapsulating the drop. Drag force on the inner or outer spheres is finally expressed as linear combinations of velocities of the three phases (i.e., the inner drop, the outer drop, and the continuous flow), respectively. Our results show that those coefficients of the linear combinations for the drag forces depend on several parameters: eccentricity of the compound drop, viscosity ratio of two neighboring phases, radius ratio of the inner drop to the outer drop, and the radius ratio of the outer drop to the tube. The two radius ratios have largest effects on the coefficients of the inner or outer drop, respectively. Stability of the compound drop in a circular tube is analyzed. It is found that though the compound drop cannot reach an absolutely steady state, it will enter a quasisteady state where the inner sphere is adjacent to the shell of the outer sphere in practice.
 [doi:10.1063/1.3460301]

I. INTRODUCTION

Mixing two immiscible fluids produces an emulsion, defined as a dispersion of droplets of one fluid in a second fluid. Emulsions play important roles in many types of processing and in coatings, cosmetics, and foods.[1] One common application is to compartmentalize one fluid in a second, which is important for packaging and stabilizing fluids and other active ingredients. The intermediate fluid forms an additional barrier that separates the innermost fluid from the outer fluid, or the continuous phase.[2] This makes double emulsions highly desirable for applications in controllable release of substances, separation, and for the control of encapsulation, release, and rheology for personal care products.[2]

The first paper on double emulsions was published by Seifriz.[3] Since then many studies have been performed for polydisperse emulsions. Usually, emulsions are produced by the two-step methods. However, any capsule formed from such double emulsions is poorly controlled in both size and structure, by nature, limiting applications that require precise control and release of active materials. Microfluidic techniques offer a better way to produce more uniform double emulsions. Utada *et al.*[2] proposed a novel microfluidic device which produces controllable monodisperse microdouble emulsions in a single step. Chu *et al.*[4] could successfully produce highly controllable double and triple emulsions by means of coflow in series of capillary tubes with coaxial calibration. They show that size and frequency of emulsions can be precisely controlled with high monodispersity by merely regulating the flow rate. Similar study was reported by Nisisako *et al.*,[5] demonstrating that microfluidic devices could generate high-monodisperse emulsions. Recent progress in this area was focused on either the experimental studies[6–8] or the numerical investigations such as Zhou *et al.*[9,10] Analytical solution of such a problem is less reported in the literature.

A classical analytical solution of rigid or fluid sphere in stationary or moving liquids in a cylindrical tube was given by Haberman and Sayre.[11] The rigid or fluid sphere does not contain inner particle or fluid sphere inside. An exact analytical solution was developed in terms of an infinite set of linear algebraic equations for the coefficients in the form of stream function. It was found that the drag force on the sphere in the tube increases exponentially as its radius increases.

Sadhal and Oguz[12] examined the low Reynolds number translatory motion of a compound drop in unbound environment. The compound drop consists of a liquid drop or a bubble fully coated by another liquid, moving in a third immiscible fluid (not confined). An analytical solution was developed for small capillary numbers by approximating the two interfaces to be spherical. The results showed that the viscous forces tend to move the inner-fluid sphere toward the front stagnation point of the compound drop. There must be a body force toward the front for equilibrium of the inner

[a]Author to whom correspondence should be addressed. Electronic mail: xjl@ncepu.edu.cn.

sphere with respect to the outer sphere. For a set of fluids, two or four equilibrium configurations may be found under gravity. Of these only one or two are stable. The others are unstable.

Oguz and Sadhal[13] studied the motion of a compound drop formed by a vapor bubble completely coated by its liquid phase in another immiscible liquid. The compound drop is growing or collapsing due to the phase change while it is translating under buoyant force. The analysis was based on the assumption of the spherical interface. An exact analytical solution was developed for the fluid-mechanical part of the problem. The heat transfer treatment of the problem requires the numerical solution if we attempt to include the convective terms with respect to time. It is found that the drag component induced by radial velocity contributes to the total drag on the bubble in eccentric configuration. This drag force is toward the center of the drop in the case of growth and has an effect of restoring concentricity. However, in the case of growth, the compound drop can not maintain its configuration of two nonintersecting eccentric spheres. In the case of collapse the bubble stays inside the drop if the collapse velocity is high enough.

Martinez and Udell[14] studied the axisymmetric creeping motion of a neutrally buoyant deformable drop flowing through a circular tube by boundary integral method. The fluids are immiscible, incompressible, and the bulk velocity is constant. The effects of the capillary number, viscosity ratio, and drop size on the deformation, drop speed, and the additional pressure loss were examined.

The motion of a compound drop in a confined environment should be different from that in unbound environment. Analytical solution of the motion of a compound drop in a circular tube is not reported in the literature. The problem studied in this paper may be encountered in various microfluidic and large scale systems. The analysis is based on the low Reynolds number Stokes flow assumption. The interface is assumed to be spherical. Stream functions in one bipolar and two cylindrical coordinate systems are given in the series form. The new contribution is the transformation between the cylindrical and bipolar coordinate systems. Drag forces are expressed as linear combinations of the three phase velocities with six coefficients. These coefficients are discussed one by one. Finally, we give the stability analysis of the compound drop.

II. STATEMENT OF THE PROBLEM

Figure 1 describes the flow system. There is a long circular tube with a radius of R_0. A compound drop is located at the centerline of the circular tube. Three immiscible, incompressible phases are labeled as 1, 2, and 3, respectively. Correspondingly, the outer radius of the compound drop is R_{23}. The inner drop has a radius of R_{12}. The compound drop, consisting of the inner and outer drops, is moving along the tube centerline. The 2-3 and 1-2 interfaces are in spherical shape with tangential mobility and translatory speed. Thus, the geometric configuration is axisymmetric. The flow rate of the continuous phase, i.e., phase 3, is constant, which can be reached in many microfluidic experiments.

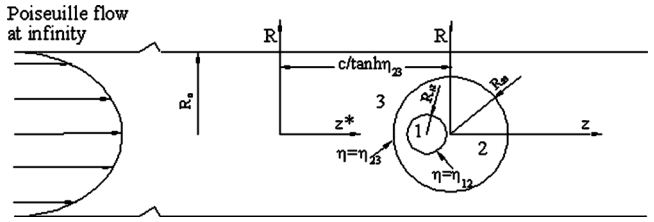

FIG. 1. The flow system of a compound drop in liquid confined by a circular tube.

The governing equations in the limit of Stokes flow are as follows:

$$\nabla \cdot \vec{u}_i = 0,$$
$$\nabla p_i = \mu_i \nabla^2 \vec{u}_i, \tag{1}$$

where the subscript i refers to the three phases, $\vec{u}_i$ is velocity vector, p is pressure, and μ is viscosity. Equation (1) is valid if the flow system is small enough so that the gravity can be neglected. Otherwise, the flow system should be positioned vertically for large flow system, under which the gravity can be incorporated into the term of p.

In this paper we totally set up two cylindrical coordinate systems and one bipolar coordinate system (η, ξ). One cylindrical coordinate system (R, z^*) is rest with respect to the circular tube. The other cylindrical coordinate system (R, z) is attached at the center of the interface 2-3. Fluid 3 moves at constant bulk velocity U relative to the interface 2-3, and interface 1-2 translates at velocity V as a whole relative to the interface 2-3. The center of interface 2-3 translates at velocity W relative to the circular tube. The boundary conditions are as follows: (i) continuity of tangential velocity at interface 2-3, (ii) zero normal velocity at interface 2-3 relative to the center of interface 2-3, (iii) continuity of shear stress at interface 2-3, (iv) continuity of tangential velocity at interface 1-2, (v) continuity of normal velocity at interface 1-2, (vi) continuity of shear stress at interface 1-2, (vii) finite velocity in phase 1, (viii) Poiseuille flow at infinity, and (ix) no-slip boundary condition at the wall of the circular tube.

The problem is completely defined by Eq. (1) and the above nine boundary conditions. The normal shear stress is automatically satisfied at large surface tension.

The process to solve the problem includes four steps in brief. Firstly, let the stream function satisfy boundary conditions (i)–(viii) under bipolar coordinate system. Second, let the stream function satisfy boundary condition (ix) under cylindrical coordinate system. Third, perform transformation of the stream function between the two coordinate systems to obtain an infinite set of liner algebra equations whose variables are coefficients of the series of the stream function. Finally, truncate the infinite equation set to be finite in order to solve. Accuracy can be elevated to any degree by retaining more equations after truncation.

In Appendices A and C, the detailed derivations for the boundary conditions under bipolar coordinate system, cylindrical coordinate system, and transformation between the two systems are elaborated.

TABLE I. Wall correction factors [1*: a solid sphere moving in a still liquid in a circular tube by Haberman and Sayre (Ref. 11); 1: present computation for case 1*; 2*: a fixed solid sphere in Poiseuille flow by Haberman and Sayre (Ref. 11); 2 (note): present computation for case 2* [note that Haberman and Sayre (Ref. 11) used the velocity at the axis of the circular tube but we use the bulk velocity of the continuous flow to define the wall correction factor; therefore, the results for 2 (note) are two times of those for 2*]; 3: present computations for $\mu_1:\mu_2:\mu_3=1:1:1$, $W:U:V=1:1:1$, $\varepsilon=0.5$, $R_{12}/R_{23}=0.5$; 4: present computations for $\mu_1:\mu_2:\mu_3=100:10:1$, $W:U:V=1:1:1$, $\varepsilon=0.75$, $R_{12}/R_{23}=0.5$; 5: present computations for $\mu_1:\mu_2:\mu_3=1:10:100$, $W:U:V=1:1:1$, $\varepsilon=0.2$, $R_{12}/R_{23}=0.5$; 6: present computations for $\mu_1:\mu_2:\mu_3=1:1:1$, $W:U:V=10:1:1$, $\varepsilon=5/6$, $R_{12}/R_{23}=0.9$].

	$\frac{R_{23}}{R_0}$								
Case	0.1	0.2	0.3	0.4	0.5	0.6	0.7	0.8	0.9
1*	1.263	1.680	2.371	3.596	5.970	11.135	24.955	73.555	N/A
1	1.2632	1.6795	2.3701	3.5914	5.9474	11.0919	24.6760	74.6700	469.2244
2*	1.255	1.635	2.231	3.218	5.004	8.651	17.671	47.301	N/A
2 (note)	2.5096	3.2696	4.4580	6.4315	9.9907	17.2260	34.9481	95.2405	532.8661
3	3.0857	3.8594	4.9823	6.6894	9.4608	14.4257	24.8441	53.9975	216.2092
4	2.9219	3.7651	5.0365	7.0512	10.4765	16.9401	31.3155	74.1093	323.3151
5	3.3669	4.0554	5.0483	6.5679	9.0830	13.7332	23.9464	54.4405	241.8377
6	2.2570	2.9100	3.9047	5.4992	8.2456	13.5023	25.3598	61.0303	268.0281

III. RESULTS AND DISCUSSION

A. Validation of the solution

As mentioned in Appendix C, the exact solution of the problem can be approached by increasing N^* (see Appendix C for definition of N^*). Our results show that $N^*=14$ leads to good accuracy for all physical properties of the three phases and most geometric configurations. Correspondingly, the solution includes 28 series terms under bipolar coordinate system. It is noted that $N^* \geq 25$ is necessary to make solution converge for very large eccentricity like 0.9, while $N^*=14$ is sufficient for eccentricity less than 0.833. Conventional floating computation still applies to cases with small and moderate eccentricity and radius ratio ($\varepsilon<0.5$, $R_{23}/R_0<0.8$), which requires small N^* and produces less abnormal linear equation set. Large numerical diffusion may be encountered in the sum and product of the recurrence formulas with increases in N^*. Besides, the coefficient matrix of the linear equation set may become abnormal if N^* is large. To ensure accuracy at large eccentricity and radius ratio, we adopt the nonstandard floating-point computation with 50-digit precision instead of 15-digit machine precision. In such a way we reach at least five-digit precision of the drag force and coefficient of the series for the extreme case ($\varepsilon=0.9$, $R_{23}/R_0=0.9$). High-precision floating-point computations with any desired precision are easily applied with mature algorithm based on integer computations, and are integrated into lots of commercial codes such as mathematical, maple, etc. Speed of the computation is acceptable unless precision is kept with hundreds of digits. Result can be obtained within minutes on an ordinary PC, which is much faster than the boundary integral method. The singularity method is impossible to provide a solution for the present problem due to the restrictions in geometry.

Due to the developed computer technology, it costs less than half minute to obtain the results with such a high accuracy for a case, using an ordinary PC with an Intel core 2 Duo E8400 CPU (3 GHz). A definition of the wall correction factor is given in Sec. III C. Wall correction factors calculated in this study for a solid sphere moving in a still liquid, and a rest solid sphere in Poiseuille flow, in a circular tube, are compared with those given by Haberman and Sayre.[11] It is observed that they match very well from Table I. The minidifference is caused by the coarse approximation of Bessel integrals by Haberman and Sayre[11] due to the limited computation resource at that time. Table I also gives the wall correction factors for some typical cases.

B. The flow field

It is found that there are four typical flow patterns for different cases (see Fig. 2). If there is no relative motion between the inner and outer spheres, flow streamlines show a set of circulation loops [see Fig. 2(a)], which are similar to the well known patterns for a single drop moving in a continuous phase. If the inner drop translates in the same direction as the continuous phase relative to the outer sphere, streamlines in the inner drop are very flat with nonuniform

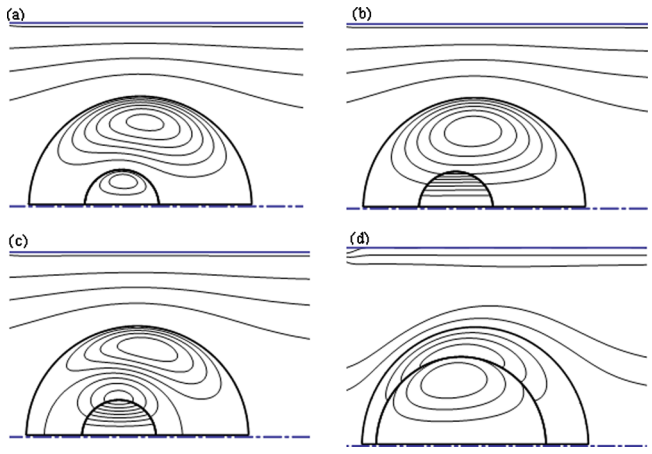

FIG. 2. (Color online) Flow patterns due to motions of inner and outer drops for $R_{23}/R_0=0.6$. (a) $\varepsilon=1/4$, $R_{12}/R_{23}=1/3$, $\mu_1:\mu_2:\mu_3=1:1:1$, $W/U=-1$, $V=0$; (b) $\varepsilon=1/4$, $R_{12}/R_{23}=1/3$, $\mu_1:\mu_2:\mu_3=1:1:1$, $W/U=1$, $V/U=1$; (c) $\varepsilon=1/4$, $R_{12}/R_{23}=1/3$, $\mu_1:\mu_2:\mu_3=1:1:1$, $W/U=1$, $V/U=-1$; (d) $\varepsilon=1/2$, $R_{12}/R_{23}=3/4$, $\mu_1:\mu_2:\mu_3=10:1:1$, $V/U=-1$, $W/U=1$.

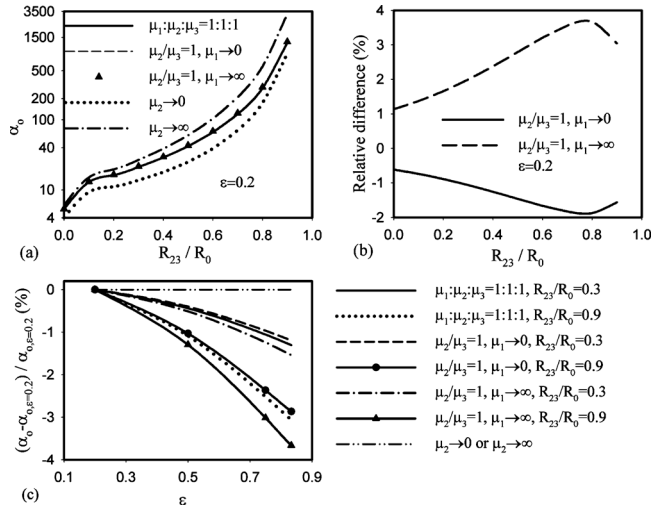

FIG. 3. Dependence of α_o on R_{23}/R_0 and eccentricity at $R_{12}/R_{23}=0.5$. (a) Variations of α_o on R_{23}/R_0. (b) Relative difference of α_o vs R_{23}/R_0, in which relative difference is defined as $(\alpha_o - \alpha_{o,\mu1:\mu2:\mu3=1:1:1,\varepsilon=0.2})/\alpha_{o,\mu1:\mu2:\mu3=1:1:1,\varepsilon=0.2}$. (c) Relative difference of α_o vs eccentricity.

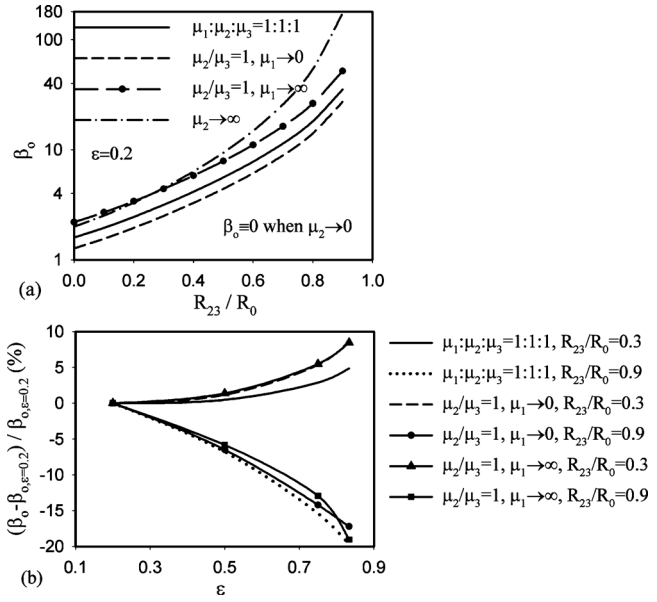

FIG. 5. Dependence of β_o on R_{23}/R_0 and ε at $R_{12}/R_{23}=0.5$. (a) β_o vs R_{23}/R_0. (b) Relative β_o vs ε.

distance between each other [see Fig. 2(b)]. Flow inside the inner drop has translatory velocity only. However, at the inner drop surface flow streamline overlaps with the surface, indicating fluid movement along the surface.

Figure 2(c) shows flow streamlines for the inner drop moving in the opposite direction with the continuous phase. Slightly curved streamlines appear inside the inner drop. There are double circulations in the outer drop beyond the inner drop. For large inner to outer drop size ratio, as shown in Fig. 2(d), circulations are complete inside the inner drop, while incomplete in the outer drop due to the limited space for the flow development.

C. Drag forces

According to Jeffery,[15] drag forces on outer and inner spheres are

$$F_o = \frac{2\sqrt{2}\mu_3\pi}{c}\sum_{n=1}^{\infty}(A_n^{(3)} + B_n^{(3)} + C_n^{(3)} + D_n^{(3)}), \tag{2}$$

$$F_i = \frac{2\sqrt{2}\mu_2\pi}{c}\sum_{n=1}^{\infty}(A_n^{(2)} + B_n^{(2)} + C_n^{(2)} + D_n^{(2)}). \tag{3}$$

Comparing Eqs. (A19) and (A21), we have

$$F_o = \frac{4\sqrt{2}\mu_3\pi}{c}\sum_{n=1}^{\infty}[A_n e^{-(n-1/2)\eta_{23}}(1-e^{-2\eta_{23}}) - (B_n + \dot{V}_1)e^{-(2n-1)\eta_{23}} - (C_n - \dot{V}_2)e^{-(2n+3)\eta_{23}}], \tag{4}$$

$$F_i = \frac{4\sqrt{2}\mu_2\pi}{c}\sum_{n=1}^{\infty} e^{-(n-1/2)\eta_{23}} \times [D_n(1-e^{-2\eta_{23}}) + E_n + F_n e^{-(n+3/2)\eta_{23}}]. \tag{5}$$

It is noted that the present problem is reduced to a simple one with a compound drop moving in a stationary unbound fluid, if the tube radius approaches infinity (consequently B_n and C_n approach zero) and $W=-U$, under which the drag force on the compound drop is called F_o^*. We define the wall correction factor Coe_{wall} as

$$Coe_{\text{wall}} = \frac{F_o}{F_o^*}. \tag{6}$$

Bulk motion of the compound drop is controlled by drag forces both on the inner and outer spheres. It is important to study the drag forces for different cases. It is seen from Eqs. (A25)–(A36) and the solution procedure of B_n and C_n that constants $A_n - G_n$ are not only linear combinations of velocity

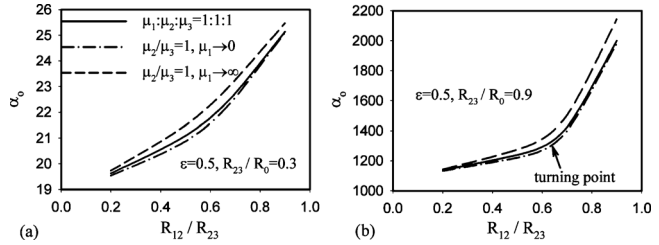

FIG. 4. Dependence of α_o on R_{12}/R_{23} at two different R_{23}/R_0 (α_o is constant when $\mu_2 \to 0$ or $\mu_2 \to \infty$ for any ε when R_{23}/R_0 is fixed).

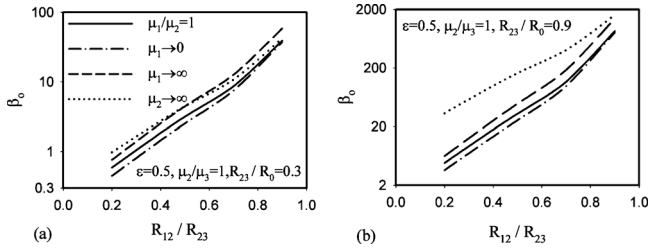

FIG. 6. β_o vs R_{12}/R_{23} for two different R_{23}/R_0 (β_o equals to zero when $\mu_2 \to 0$).

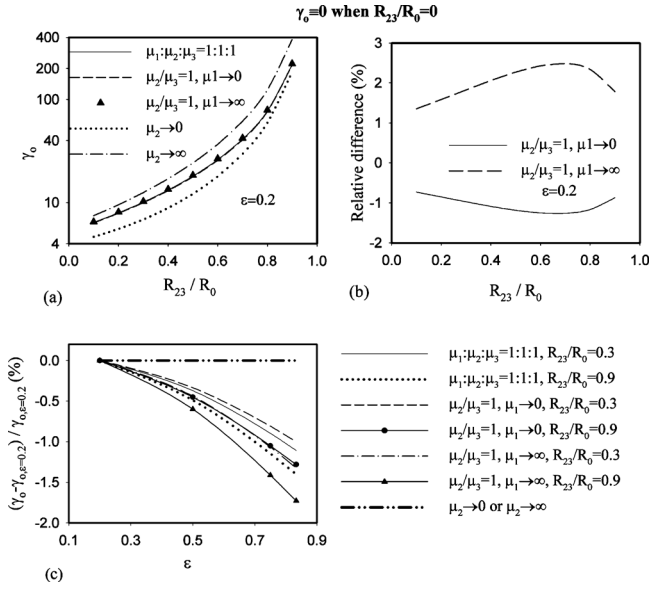

FIG. 7. Dependence of γ_o on R_{23}/R_0 and eccentricity at $R_{12}/R_{23}=0.5$. (a) Variations of γ_o on R_{23}/R_0. (b) Relative difference of γ_o vs R_{23}/R_0, in which relative difference is defined as $(\gamma_o - \gamma_{o,\mu1:\mu2:\mu3=1:1:1,\varepsilon=0.2})/\gamma_{o,\mu1:\mu2:\mu3=1:1:1,\varepsilon=0.2}$. (c) Relative difference of γ_o vs eccentricity.

$2W+U$, $W+U$, and V, but also proportional to the drop radius and viscosity of the phase encapsulating the drop. Thus, by Eqs. (4) and (5) we obtain

$$F_o = (\alpha_o W + \beta_o V + \gamma_o U)\pi\mu_3 R_{23}, \tag{7}$$

$$F_i = (\alpha_i W + \beta_i V + \gamma_i U)\pi\mu_2 R_{12}, \tag{8}$$

where α_o, β_o, γ_o, α_i, β_i, and γ_i are coefficients for W, V, and U, respectively. The subscripts o and i represent the outer and inner spheres. These coefficients depend on geometric configuration $(R_{23}/R_0, R_{12}/R_{23}, \varepsilon)$ and viscosity ratio $(\mu_1/\mu_3, \mu_2/\mu_3)$.

Figures 3 and 4 show variations of α_o dependent on R_{12}/R_{23}, R_{23}/R_0, ε, and viscosity ratios of the three phases. As seen from Fig. 3(a), α_o increases significantly with increases in R_{23}/R_0. This trend becomes more apparent when the outer sphere radius approaches the radius of the circular tube, i.e., $R_{23}/R_0 \to 0$. For instance, α_o at $R_{23}/R_0=0.9$ is several hundred times larger than that at $R_{23}/R_0=0$, causing very high wall correction factors. Effects of viscosity ratios μ_1/μ_2 and μ_2/μ_3 on α_o are different. It is interesting to find that α, β, and γ at $\mu_3 \to 0$ are the same as those at $\mu_2 \to \infty$.

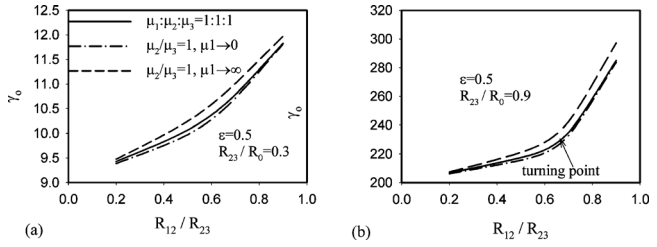

FIG. 8. Dependence of γ_o on R_{12}/R_{23} at two different R_{23}/R_0 (γ_o is constant when $\mu_2 \to 0$ or $\mu_2 \to \infty$ for any ε when R_{23}/R_0 is fixed).

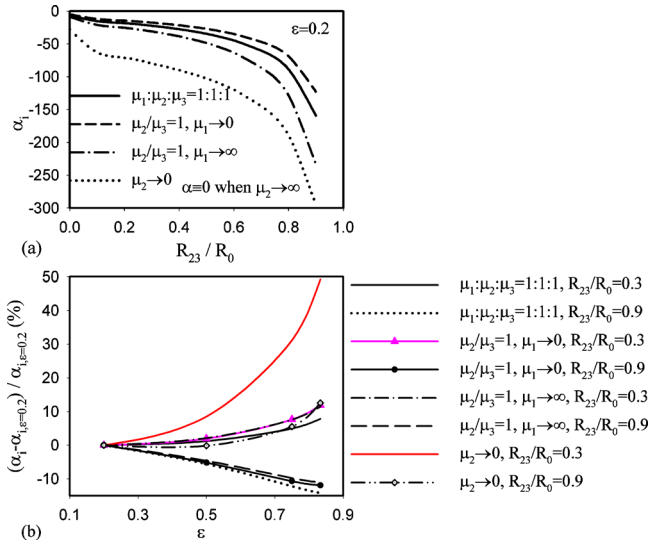

FIG. 9. (Color online) α_i vs R_{23}/R_0 and ε at $R_{12}/R_{23}=0.5$, $\alpha_i \equiv 0$ when $\mu_2 \to \infty$. (a) α_i vs R_{23}/R_0. (b) Relative α_i vs ε.

Meanwhile, these coefficients are identical at $\mu_3 \to \infty$ and $\mu_2 \to 0$, no matter how μ_1 changes. Two special cases of $\mu_2 \to 0$ and $\mu_2 \to \infty$ give the lower and upper bounds of α_o for all viscosity ratios, corresponding to gas bubble and solid sphere for phase 2, respectively. Because the three curves $(\mu_1:\mu_2:\mu_3=1;\ \mu_1 \to 0,\ \mu_2:\mu_3=1;$ and $\mu_1 \to \infty,\ \mu_2:\mu_3=1)$ in Fig. 3(a) nearly overlap, relative difference of α_o from the case of $\mu_1:\mu_2:\mu_3=1$ is given in Fig. 3(b), indicating the maximum difference of less than 4%. Figures 3(a) and 3(b) show that the inner drop viscosity μ_1 has very small effect on α_o. Besides, the eccentricity has mini-influence on α_o [see Fig. 3(c)]. It is noted that α_o has nothing to do with eccentricity when phase 2 is gas bubble or solid sphere.

We consider the effect of radius ratio of inner drop to outer drop, i.e., R_{12}/R_{23}, on α_o in Fig. 4. α_o is increased with increases in R_{12}/R_{23}, see Fig. 4(a) for small radius ratio of outer drop to circular tube $(R_{23}/R_0=0.3)$. For large R_{23}/R_0 such as 0.9, slopes of α_o versus R_{12}/R_{23} become large when R_{12}/R_{23} is larger than a critical value about 0.7 [see Fig. 4(b)]. Generally, α_o increases significantly with increases in R_{23}/R_0 by comparing Figs. 4(a) and 4(b).

In general, the effect of β_o on the drag force is smaller than α_o by comparing Figs. 4 and 5. Viscosity ratios of the three phases have a complicated influence on β_o. As shown in Fig. 5(a), β_o is zero when the outer sphere is gas bubble $(\mu_2 \to 0)$, giving the lower bound of β_o among all the viscosity ratios. However, β_o with solid outer sphere $(\mu_2 \to \infty)$ does

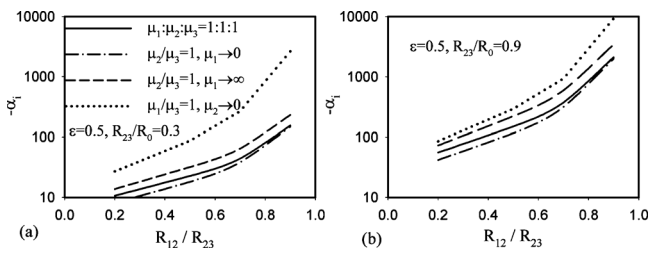

FIG. 10. $-\alpha_i$ vs R_{12}/R_{23} at two different R_{23}/R_0, $\alpha_i \equiv 0$ when $\mu_2 \to \infty$.

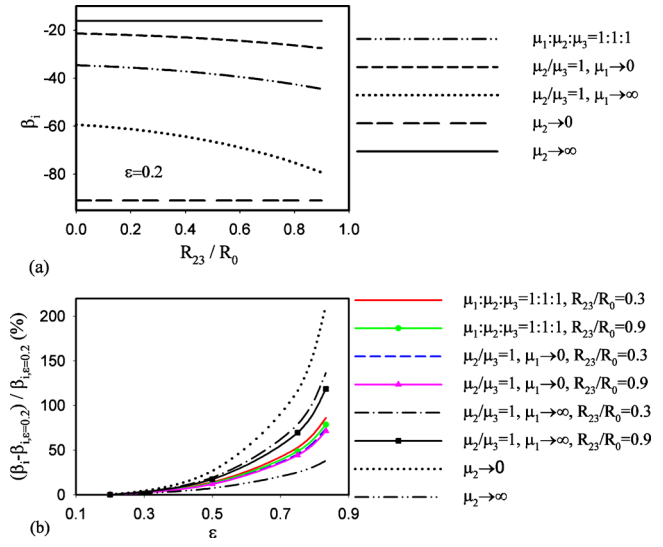

FIG. 11. (Color online) β_i vs R_{23}/R_0 and ε at $R_{12}/R_{23}=0.5$. (a) β_i vs R_{23}/R_0. (b) Relative β_i vs ε.

not give the upper bound. For instance, β_o with solid outer sphere ($\mu_2 \to \infty$) is even slightly smaller than that at $\mu_2/\mu_3 = 1$ and $\mu_1 \to \infty$ for R_{23}/R_0 smaller than 0.4 [see Fig. 5(a)]. Eccentricity has a larger effect on β_o than on α_o by comparing Figs. 3(c) and 5(b), due to the closer relationship between eccentricity and V than the relationship between eccentricity and W, where V is the inner drop velocity relative to the outer sphere, and W is the continuous phase velocity relative to the outer sphere. Moreover, two contrary trends are observed for α_o versus ε, i.e., α_o increases as ε increases at lower R_{23}/R_0, but α_o decreases as ε increases at higher R_{23}/R_0, as shown in Fig. 5(b).

Figure 6 shows β_o versus R_{12}/R_{23} (radius ratio of inner sphere to outer sphere) at two different R_{23}/R_0 of 0.3 and 0.9. Both subfigures give the increased β_o with increases in R_{12}/R_{23}.

It is shown in Figs. 7 and 8 that γ_o exhibits similar dependence on the parameters R_{12}/R_{23}, R_{23}/R_0, and ε. γ_o increases fast as R_{12}/R_{23} or R_{23}/R_0 approaches unity. However, γ_o contributes much less to the drag force on the outer drop, especially when R_{12}/R_{23} or R_{23}/R_0 is close to unity, indicating that relative movement between the drop and bulk flow of the continuous phase dominates over the drag force. Therefore, drag force on the outer drop is far more sensitive to W than U.

α_i and β_i are negative for all the cases, indicating deviation of the inner drop from the centroid of the compound drop. As shown in Fig. 9(a), α_i at $\mu_2 \to 0$ and $\mu_2 \to \infty$ give the low and up bounds among all viscosity ratios of the three phases. Eccentricity ε has larger influence on α_i than on α_o by comparing Figs. 3(c) and 9(b). It is observed from Fig. 9(b) that α_i can be increased or decreased with increases in eccentricities, depending on viscosity ratios of three phases and R_{23}/R_0. Figure 10 shows that $-\alpha_i$ is increased exponentially with increases in R_{12}/R_{23}. This is true no matter how other parameters change.

β_i represents the drag force on the inner drop due to the inner sphere velocity V relative to the outer sphere. Figure

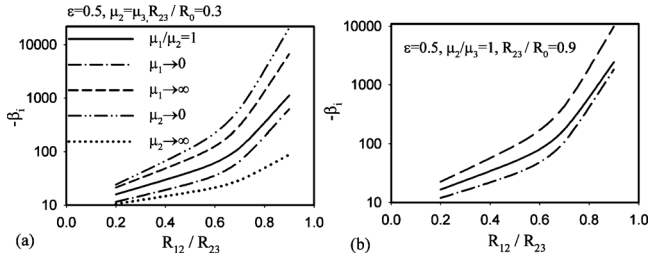

FIG. 12. β_i vs R_{12}/R_{23} at two different R_{23}/R_0 (β_i is constant if $\mu_2 \to 0$ or $\mu_2 \to \infty$).

11(a) illustrates that β_i is quite insensitive to R_{23}/R_0. This is because the geometry parameter outside the compound drop has almost nothing to do with the drag force on the inner sphere. Figure 11(b) shows that β_i increases monotonically with increases in eccentricity. Slopes of β_i versus ε become very large when ε approaches unity.

Similar to Fig. 10 for α_i versus R_{12}/R_{23}, Fig. 12 shows that $-\beta_i$ is increased exponentially with increases in R_{12}/R_{23}. For smaller R_{12}/R_{23} such as less than 0.2, gradient of $-\beta_i$ versus R_{12}/R_{23} is not large, under which R_{12}/R_{23} is not the dominant parameter contributing to the drag force on the inner drop. For larger R_{12}/R_{23}, however, slope of $-\beta_i$ versus R_{12}/R_{23} is tremendously high, indicating that the drag force on the inner sphere is dominated by R_{12}/R_{23}.

In general, γ_i is sensitive to ε, as shown in Fig. 13(b). Unlike α_i, the absolute value of γ_i increases rapidly with the increase of ε in all the cases studied, and is very insensitive to R_{23}/R_0, as demonstrated, respectively, in Figs. 13(a) and 14. Although γ_i becomes larger as R_{12}/R_{23} increases from 0.1 to 0.9, it is still far smaller compared with α_i and β_i at the same condition. As a result, γ is taken much less important compared with α and β. It is easy to understand since γ is associated with the relative velocity U toward the tube wall, which has less relationship to the flow resistance exerted on the drop.

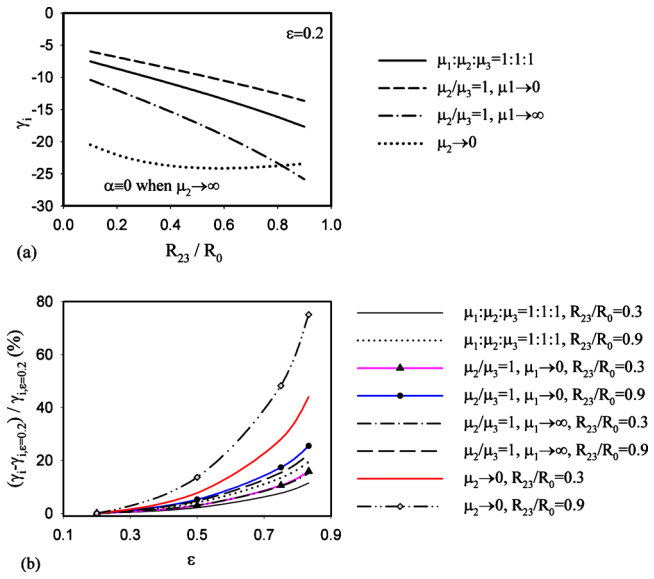

FIG. 13. (Color online) γ_i vs R_{23}/R_0 and ε at $R_{12}/R_{23}=0.5$, $\alpha_i \equiv 0$ when $\mu_2 \to \infty$. (a) γ_i vs R_{23}/R_0. (b) Relative γ_i vs ε.

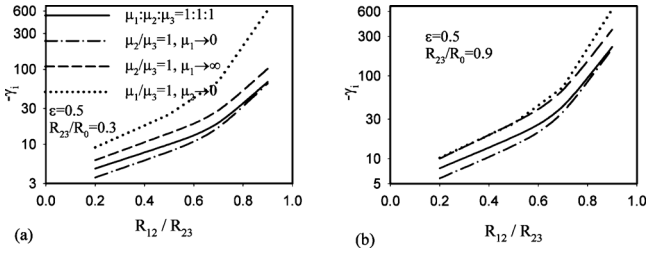

FIG. 14. $-\gamma_i$ vs R_{12}/R_{23} at two different R_{23}/R_0, $\gamma_i \equiv 0$ when $\mu_2 \to \infty$.

D. Validation of spherical shape assumption

As indicated above, drag forces increase significantly when R_{12}/R_{23} and R_{23}/R_0 approach unity. One may concern the condition under which the spherical phase shape is valid. Note that exact spherical shape is never reached because it is impossible to satisfy the normal stress boundary condition everywhere on the sphere surface with limited interfacial tension. This is easily inferred from the normal stress boundary condition to be satisfied, which is neglected and treated to be automatically satisfied with infinite surface tension in the above sections. Normal stress on sphere surface is expressed as $\omega = -p + 2\mu(\partial u/\partial \eta)$ in bipolar coordinate system. Thus, normal stress on inner and outer spheres should satisfy the following equations, respectively:

$$\omega_2 = -p_2 + 2\mu_2 \frac{\partial u_{\eta,2}}{\partial \eta} \equiv \omega_1 - p_1 + 2\mu_1 \frac{\partial u_{\eta,1}}{\partial \eta} + \frac{2\tau_{12}}{R'_{12}}, \quad (9a)$$

$$\omega_3 - p_3 + 2\mu_3 \frac{\partial u_{\eta,3}}{\partial \eta} \equiv \omega_2 - p_2 + 2\mu_2 \frac{\partial u_{\eta,2}}{\partial \eta} + \frac{2\tau_{23}}{R'_{23}}, \quad (9b)$$

where subscripts 1, 2, and 3 denote the three fluids while τ_{12} and τ_{23} denote interfacial tensions for the two spherical surfaces. R'_{23} and R'_{12} are local curvature radii of the outer and inner surfaces. The stress jump $\Delta\omega_{12} = 2\tau_{12}/R'_{12}$ and $\Delta\omega_{23} = 2\tau_{23}/R'_{23}$ across the two interfaces are determined by interfacial tensions. Although the absolute value of $\Delta\omega$ increases as interfacial tension increases, the difference of $\Delta\omega$ between any pair points on the sphere is uniquely determined by a given flow status. Therefore it is obvious that R'_{23} and R'_{12} approach R_{23} and R_{12}, respectively, as interfacial tensions τ_{12} and τ_{23} approach infinity. From the practical point of view, the spherical interface assumption is valid if the local curvature radius has small variance such as 10% or 5% across the whole interface. We have the following two equations when subscripts 12 and 23 are omitted for simplicity:

$$\Delta\omega_{\max} = \frac{2\tau}{R - \Delta R^-}, \quad (10a)$$

$$\Delta\omega_{\min} = \frac{2\tau}{R + \Delta R^+}, \quad (10b)$$

where ΔR^+ and ΔR^- represent maximum positive and negative curvature radii deviating from R at the limit of τ approaching infinity. Therefore, $R - \Delta R^-$ and $R + \Delta R^+$ represent the minimum and maximum local curvature radii of the drop surface, respectively. It is sure that ΔR must be small compared to R in order to form spherical shape for the drop. Thus, Eq. (11) is inferred from Eq. (10) that

$$\Delta\omega_{\max} - \Delta\omega_{\min} = \frac{2\tau(\Delta R^+ + \Delta R^-)}{(R - \Delta R^-)(R + \Delta R^+)} \approx \frac{2\tau(\Delta R^+ + \Delta R^-)}{R^2}. \quad (11)$$

Thus, the degree of maximum shape deformation ΔS from the real drop to fluid sphere is written as follows:

$$\Delta s = \frac{\Delta R^+ + \Delta R^-}{2} \Big/ R \times 100\% \approx \frac{(\Delta\omega_{\max} - \Delta\omega_{\min})R}{4\tau} \times 100\%. \quad (12)$$

By verifying the small value of Δs (e.g., 10% or 5%), we can assess whether the assumption of spherical shape is applicable. Several typical flow conditions are examined in microfluidic regime, as illustrated in Fig. 15. Pressure p is evaluated from the stream function following the complex procedure provided by Pasol *et al.*[16] It is found that p has similar expression as stream function: it is proportional to μ and is a linear combination of U, V, and W. According to Eq. (12), Δs is in inverse to surface tension τ, so it is in proportion to capillary number Ca. It is difficult to pinpoint where $\Delta\omega_{\max}$ and $\Delta\omega_{\min}$ appear on the drop surface due to difficulty to find the zero-points of the derivatives of the nonlinear partial equations. Therefore, we calculate 12 points equally distributed on each sphere surface and perform comparison to find the approximate maximum and minimum surface stress jump among these points. Two capillary numbers are defined in Fig. 15, $\mathrm{Ca}_o = \mu_3 W/\tau_{23}$ for the outer drop and $\mathrm{Ca}_i = \mu_2 W/\tau_{12}$ for the inner drop. Figure 15(a) shows the degree of maximum shape deformation with several typical microfluidic running parameters. When R_{23}/R_0 and R_{12}/R_{23} are less than 0.5, Δs is around or less than 10% at

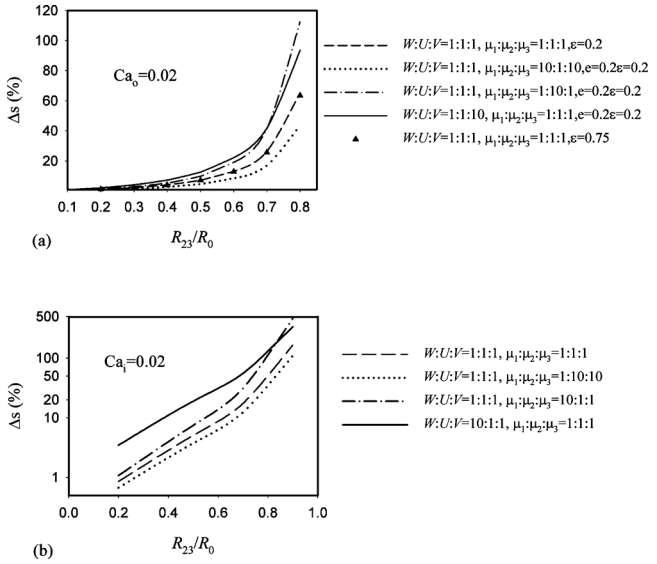

FIG. 15. Maximum variation of local curvature radius of surfaces of outer and inner spheres, (a) for outer sphere and (b) for inner sphere

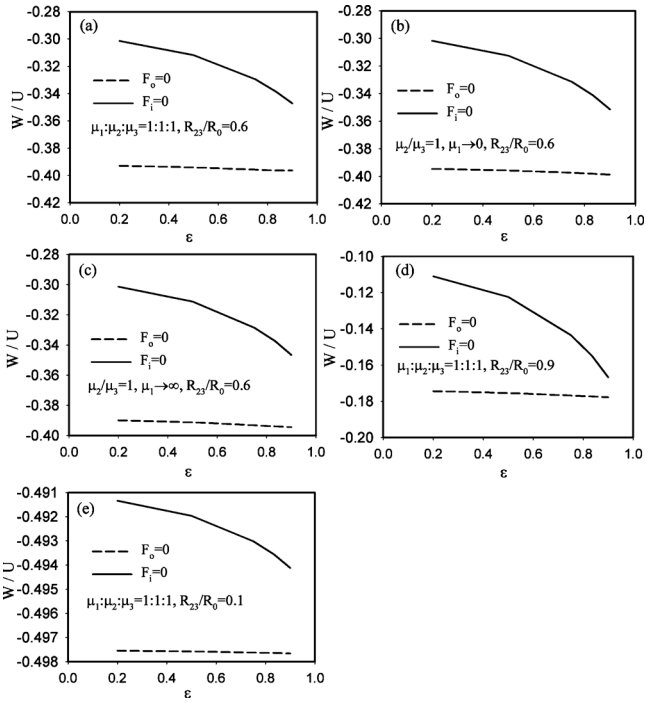

FIG. 16. Stability region for a compound drop in a long circular tube at various conditions.

$\mathrm{Ca}_o=0.025$ and $\mathrm{Ca}_i=0.025$ for different values of viscosity ratio and eccentricity. Note that shape deformation varies in proportion to the Ca number. Therefore, the assumption of spherical shape is valid with even larger radius ratios in micro- or nanosystems where capillary number can reach as low as 10^{-4}. Since the capillary number in most microfluidic systems is smaller than 10^{-2}, we conclude that analytical solution is applicable with moderate radius ratio such as R_{23}/R_0 and R_{12}/R_{23} are less than 0.6.

E. Stability analysis

Gravity is not important in fluid mechanics for small size flow systems. Thus, we focus on the situation under which the flow system is horizontally positioned. For Stokes flow in large scale systems, Sadhal and Oguz[12] studied the flow for which gravity induced buoyancy is important to sustain steady vertical movement of a compound drop. When a steady state of a compound drop is reached, drag forces on both inner and outer spheres disappear. Besides, there is no relative motion between the inner and outer spheres ($V=0$). Thus, we have

$$F_o = \alpha_o W + \gamma_o U = 0 \rightarrow \frac{W}{U} = -\frac{\gamma_o}{\alpha_o}, \tag{13}$$

$$F_i = \alpha_i W + \gamma_i U = 0 \rightarrow \frac{W}{U} = -\frac{\gamma_i}{\alpha_i}. \tag{14}$$

We plot curves of $-\gamma_o\alpha_o$ (dashed curves) and $-\gamma_i/\alpha_i$ (solid curves) against eccentricity ε in Fig. 16. The two curves represent $F_o=0$ and $F_i=0$, respectively. Velocity ratios of W/U can be varied anywhere in Fig. 16. Steady state of a compound drop can be reached if the two curves intersect

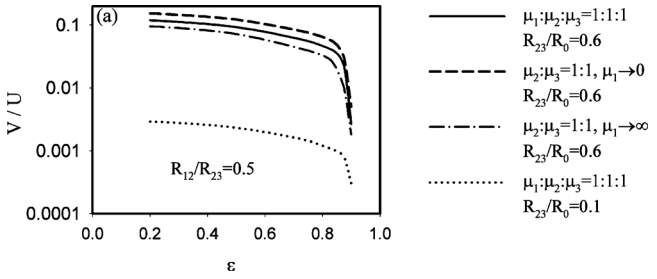

FIG. 17. Inner/outer velocity ratio when drag forces disappear.

with each other. It is observed from Fig. 16 that the two curves approach each other as ε increases. However, they never intersect, indicating that the absolutely steady state can not be reached, even at very large eccentricity. The inner droplet will eventually collide with the outer drop. This is true for all the cases studied in this paper.

On the other hand, collision of the drops does not necessarily imply breakage of the compound drop. Moreover, the compound drop may travel over a long range through the tube before collision occurs. As is seen from Fig. 16, although the two curves representing $F_o=0$ and $F_i=0$, respectively, do not intersect under the condition that V is zero, they do sit close to each other, especially when ε approaches unity. There is no solution for force-free state of the two drops if V is zero, i.e., the compound drop cannot reach static equilibrium. The inner and outer drops can reach a force-free state simultaneously if V is not zero. The instantaneous balance will be broken after the geometric configuration changes due to the nonzero V. If V is relatively small, however, the force-free state of the inner and the outer drops may be reinstated rapidly due to the slow change of the geometric configuration. This process is in analogy to an inflating fire balloon: the pressure outsize and inside the balloon cannot be balanced if the balloon is inflating rapidly, whereas the quasistatic state is reached when the balloon is inflating very slowly. The problem is that the compound drop can not be stable for a long time with ε close to unity, as observed in many experiments, supported by the finding that the drag forces are zero when V is small.

Replacing Eqs. (13) and (14) with Eqs. (15) and (16), we obtain

$$F_o = \alpha_o W + \beta_o V + \gamma_o U = 0, \tag{15}$$

$$F_i = \alpha_i W + \beta_i V + \gamma_i U = 0. \tag{16}$$

From Eqs. (15) and (16) we obtain

$$V = \frac{\alpha_o\gamma_i - \alpha_i\gamma_o}{\alpha_i\beta_o - \alpha_o\beta_i} U. \tag{17}$$

By Eq. (17) we can plot the ratio of V to U against eccentricity ε, as shown in Fig. 17. Because the value of V/U is symmetric against the straight line of $\varepsilon=0$, the curve is only plotted for ε from 0 to 1. It is observed that the relative motion between the inner sphere and outer sphere is very weak compared with velocity of the outer drop to the tube wall. For example, when the inner drop is located near the center of the compound drop, the relative velocity between

the inner and outer spheres is about only one tenth of the bulk velocity of the compound drop to yield the zero total forces on the inner and compound drop. Moreover, the velocity V decreases dramatically as ε approaches 0.9. Therefore, we can expect the compound drop to reach a kind of quasisteady state where joined forces on inner and outer spheres vanish. Besides, the inner drop is almost at rest when it is located near the shell of the outer drop. It means that stable compound drops can be produced in laboratory because it costs relatively short time for a compound drop to move in the tube. Since drag forces and V/U are symmetric to the line $\varepsilon=0$, whether final location of the inner drop is near $\varepsilon=1$ or $\varepsilon=-1$ is determined by the initial conditions.

Although the compound drop can not reach an absolutely steady state, it will enter a quasisteady state when the inner sphere is adjacent to the shell of the outer sphere. Nonaxisymmetric disturbance and/or configuration cause the compound drop deviating from the centerline of the tube. This is because it is hard to produce perfectly axisymmetric coflow in practice. It is difficult to reach an analytical solution for the nonaxisymmetric compound drop problem, but it may be treated for small deviation of the drop from the centerline of the tube, which needs future work.

IV. CONCLUSION

An exact analytical solution was developed for the motion of a compound drop in a long circular tube. Three phases are involved in the problem, which can be encountered in various microfluidic devices to produce double emulsions. The analysis is based on the low Reynolds number Stokes flow theory. Stream functions in one bipolar and two cylindrical coordinate systems are developed in series forms. Our new contribution focuses on the transformation between the cylindrical and bipolar coordinate systems. Flow field in the whole computation domain can be obtained through the developed stream functions. Flow patterns are mainly dependent on the relative motion and the size of the inner drop. Four types of flow patterns are identified. Drag forces on the inner and outer spheres are expressed as linear combinations of velocities of the three phases with six coefficients α_i, β_i, γ_i, α_o, β_o, and γ_o. Drag force on the inner or outer spheres is in proportion to the sphere radius and viscosity of the phase encapsulating the drop. Our results show that coefficients α_i, β_i, γ_i, α_o, β_o, and γ_o for drag forces depend on various parameters such as viscosity ratio, radius ratio, and eccentricity, among which R_{12}/R_{23} and R_{23}/R_0 have the largest effect on the coefficients for the inner or outer drop, respectively. Finally, we analyze the stability of the compound drop in a circular tube. We found that although the compound drop cannot reach an absolutely steady state, it will enter a quasisteady state where the inner drop is adjacent to the shell of the outer drop in practice. At present, the analytical solution is limited to axisymmetric configuration which idealizes the experimental setup, and future work is expected to be done to tackle the nonasymmetric problem.

ACKNOWLEDGMENTS

The work is supported by the National Natural Science Foundation of China with Contract No. 50825603.

APPENDIX A: THE BIPOLAR COORDINATE SYSTEM

By carrying out the transformation,

$$R = c\frac{\sin\xi}{\cosh\eta - \cos\xi}, \quad z^* = c\frac{\sinh\eta}{\cosh\eta - \cos\xi}, \tag{A1}$$

we establish the relationship between the bipolar coordinate system and the cylindrical coordinate system at rest relative to the circular tube, where c is one half the distance between the points defined by $\eta\to\infty$ and $\eta\to-\infty$. Under bipolar coordinate system, constant values of η represent a set of nonintersecting eccentric spheres. We identify the inner sphere by $\eta=\eta_{12}$ and the outer sphere by $\eta=\eta_{23}$. Setting R_{12} and R_{23} as the radii of the spheres, R_0 as the cylinder radius, d as the distance between the centers of the two spheres (see Fig. 1), and ε as the eccentricity, we have

$$R_{23} = \frac{c}{\sinh\eta_{23}}, \quad R_{12} = \frac{c}{\sinh\eta_{12}}, \quad \text{and} \quad \varepsilon = \frac{d}{R_{23}-R_{12}}. \tag{A2}$$

By applying a little algebra, we obtain the following expressions about η_{12} and η_{23}:

$$\eta_{12} = \operatorname{arccosh}\frac{R_{23}^2 - R_{12}^2 - d^2}{2dR_{12}},$$
$$\eta_{23} = \operatorname{arccosh}\frac{d^2 + R_{23}^2 - R_{12}^2}{2dR_{23}}. \tag{A3}$$

Combining Eqs. (A2) and (A3), the coordinate constant c can be determined. It is noted that η_{12}, η_{23}, and d have the same sign. For the case that the compound drop moves with negative η_{12}, η_{23}, and d, there is a mirror against which another compound drop is symmetrical to the $\eta=0$ plane with positive η_{12}, η_{23}, and d, moving in opposite direction. Therefore, for the analysis simplicity, we only deal with the case that the compound drop lies on the $\eta>0$ area with positive η_{12}, η_{23}, and d, unless it is emphasized for the negative values of η in this paper.

By introducing stream function $\Psi^{(i)}(\eta,\xi)$ which satisfies the expression of

$$(u_\eta, u_\xi) = \frac{(\cosh\eta - \cos\xi)^2}{c^2\sin\xi}\left(\frac{\partial\Psi}{\partial\xi}, -\frac{\partial\Psi}{\partial\eta}\right), \tag{A4}$$

Eq. (1) can be transformed into

$$D^2(\Psi^{(i)}) = 0, \tag{A5}$$

where the subscript i refers to the three phases, operator D satisfies[15]

$$D=\frac{\sin\xi(\cosh\eta-\cos\xi)}{c^2}\left[\frac{\partial}{\partial\eta}\left(\frac{\cosh\eta-\cos\xi}{\sin\xi}\right)\frac{\partial}{\partial\eta}+\frac{\partial}{\partial\xi}\left(\frac{\cosh\eta-\cos\xi}{\sin\xi}\right)\frac{\partial}{\partial\xi}\right]. \tag{A6}$$

Boundary conditions (i)–(viii) can be expressed in bipolar coordinate system as

$$\left.\frac{\partial\Psi^{(3)}}{\partial\eta}\right|_{\eta=\eta_{23}}=\left.\frac{\partial\Psi^{(2)}}{\partial\eta}\right|_{\eta=\eta_{23}}, \tag{A7}$$

$$\Psi^{(3)}|_{\eta=\eta_{23}}=\Psi^{(2)}|_{\eta=\eta_{23}}=0, \tag{A8}$$

$$\mu_3 T(\Psi^{(3)})|_{\eta=\eta_{23}}=\mu_2 T(\Psi^{(2)})|_{\eta=\eta_{23}}, \tag{A9}$$

where operator T is expressed as[12]

$$T=\frac{1}{c^3}\left\{\frac{\partial}{\partial\xi}\left[\frac{(\cosh\eta-\cos\xi)^3}{\sin\xi}\right]\frac{\partial}{\partial\xi}-\frac{\partial}{\partial\eta}\left[\frac{(\cosh\eta-\cos\xi)^3}{\sin\xi}\right]\frac{\partial}{\partial\eta}\right\}, \tag{A10}$$

$$\left.\frac{\partial\Psi^{(2)}}{\partial\eta}\right|_{\eta=\eta_{12}}=\left.\frac{\partial\Psi^{(1)}}{\partial\eta}\right|_{\eta=\eta_{12}}, \tag{A11}$$

$$\Psi^{(2)}|_{\eta=\eta_{12}}=\frac{1}{2}Vc^2\frac{\sin^2\xi}{(\cosh\eta_{12}-\cos\xi)^2}=\Psi^{(1)}|_{\eta=\eta_{12}}, \tag{A12}$$

$$\mu_2 T(\Psi^{(2)})|_{\eta=\eta_{12}}=\mu_1 T(\Psi^{(1)})|_{\eta=\eta_{12}}, \tag{A13}$$

$$\Psi^{(1)}|_{\eta\to\infty}<\infty, \tag{A14}$$

$$\Psi^{(3)}|_{\eta,\xi\to0}=\frac{(2W+U)c^2\sin^2\xi}{2(\cosh\eta-\cos\xi)^2}-\frac{(W+U)c^4\sin^4\xi}{2(\cosh\eta-\cos\xi)^4R_0^2}. \tag{A15}$$

In Eqs. (A12) and (A15), the parameters V, W, and U are relative velocities to the inner sphere, outer sphere, and Poiseuille flow. The boundary condition (ix) is to be determined in Appendix B

Jeffery[15] gave a general solution for an axisymmetric problem under bipolar coordinate system, which was written as

$$\Psi^{(i)}=(\cosh\eta-\cos\xi)^{-3/2}\sum_{n=-1}^{\infty}\Theta_n^{(i)}C_{n+1}^{-1/2}(\cos\xi), \tag{A16}$$

where $C_{n+1}^{-1/2}$ is the Gegenbauer polynomial of order $(n+1)$ and degree of $-1/2$. $\Theta_n^{(i)}$ is denoted as

$$\Theta_n^{(i)}=A_n^{(i)}\left[\cosh\left(n-\tfrac{1}{2}\right)\eta\right]+B_n^{(i)}\left[\sinh\left(n-\tfrac{1}{2}\right)\eta\right]+C_n^{(i)}\times\left[\sinh\left(n-\tfrac{1}{2}\right)\eta\right]+D_n^{(i)}\left[\sinh\left(n+\tfrac{3}{2}\right)\eta\right], \tag{A17}$$

where $A_n^{(i)}$–$D_n^{(i)}$ represent the 12 integration constants. In this study, the first two terms in the series of Eq. (A16) should be omitted due to the finite velocity at $R=0$ and the symmetry flow to the centerline of the circular tube. Thus, Eq. (A16) becomes

$$\Psi^{(i)}=(\cosh\eta-\cos\xi)^{-3/2}\sum_{n=1}^{\infty}\Theta_n^{(i)}C_{n+1}^{-1/2}(\cos\xi). \tag{A18}$$

Solutions of $\Theta_n^{(i)}$ satisfying Eqs. (A8), (A12), (A14), and (A15) are written as Eqs. (A19)–(A22), which contain seven integration constants denoted as A_n, B_n, C_n, D_n, E_n, F_n, and G_n (A_n–D_n are not the alternative form for $A_n^{(i)}$–$D_n^{(i)}$!),

$$\Theta_n^{(3)}=\sqrt{2}(n+1)nc^2\left\{\frac{W+\frac{U}{2}+\frac{2}{3}c^2R_0^{-2}(n-1)(n-2)(W+U)}{2n-1}[e^{-(n-1/2)\eta}-e^{(n-1/2)(\eta-2\eta_{23})}]-\frac{W+\frac{U}{2}+\frac{2}{3}c^2R_0^{-2}(n+3)(n+2)(W+U)}{2n+3}[e^{-(n+3/2)\eta}-e^{(n+3/2)(\eta-2\eta_{23})}]+A_n[e^{(n-1/2)(\eta-\eta_{23})}-e^{(n+3/2)(\eta-\eta_{23})}]+B_n[e^{-(n-1/2)\eta}-e^{(n-1/2)(\eta-2\eta_{23})}]+C_n[e^{-(n+3/2)\eta}-e^{(n+3/2)(\eta-2\eta_{23})}]\quad(\eta>0), \tag{A19}$$

$$\Theta_n^{(3)}=\sqrt{2}(n+1)nc^2\left\{\frac{W+\frac{U}{2}+\frac{2}{3}c^2R_0^{-2}(n-1)(n-2)(W+U)}{2n-1}[e^{(n-1/2)\eta}-e^{(n-1/2)(\eta-2\eta_{23})}]-\frac{W+\frac{U}{2}+\frac{2}{3}c^2R_0^{-2}(n+3)(n+2)(W+U)}{2n+3}[e^{(n+3/2)\eta}-e^{(n+3/2)(\eta-2\eta_{23})}]+A_n[e^{(n-1/2)(\eta-\eta_{23})}-e^{(n+3/2)(\eta-\eta_{23})}]+B_n^*e^{(n-1/2)\eta}-B_ne^{(n-1/2)(\eta-2\eta_{23})}+C_n^*e^{(n+3/2)\eta}-C_ne^{(n+3/2)(\eta-2\eta_{23})}\quad(\eta<0). \tag{A20}$$

Equation (A20) is deducted based on expansions of the term of $R^{2L}z^m$ for $\eta<0$ in Appendix B, and it is useless because we only consider that the case for $\eta>0$ is given only for the sake of integrity of the whole flow field of phase 3,

$$\Theta_n^{(2)} = D_n\left\{\cosh\left[\left(n-\frac{1}{2}\right)(\eta-\eta_{23})\right] - \cosh\left[\left(n+\frac{3}{2}\right)(\eta-\eta_{23})\right]\right\} + E_n\sinh\left[\left(n-\frac{1}{2}\right)(\eta-\eta_{23})\right] + F_n\sinh\left[\left(n+\frac{3}{2}\right)(\eta-\eta_{23})\right], \tag{A21}$$

$$\Theta_n^{(1)} = \frac{\sqrt{2}}{2}Vc^2(n+1)n\left[\frac{e^{-(n-1/2)\eta}}{2n-1} - \frac{e^{-(n+3/2)\eta}}{2n+3}\right] + G_n[e^{-(n-1/2)(\eta-\eta_{12})} - e^{-(n+3/2)(\eta-\eta_{12})}]. \tag{A22}$$

In order to satisfy Eqs. (A19), (A20), and (A22), the following two identities are applied:

$$\frac{\sin^2\xi}{(\cosh\eta-\cos\xi)^{1/2}} = \sqrt{2}\sum_{n=1}^{\infty}(n+1)n\left[\frac{e^{\pm(n-1/2)\eta}}{2n-1} - \frac{e^{\pm(n+3/2)\eta}}{2n+3}\right]\cdot C_{n+1}^{-1/2}(\cos\xi), \tag{A23}$$

$$\frac{\sin^4\xi}{(\cosh\eta-\cos\xi)^{5/2}} = \frac{4\sqrt{2}}{3}\sum_{n=1}^{\infty}\left[\frac{(n+2)(n+3)e^{\pm(n+3/2)\eta}}{2n+3} - \frac{(n-1)(n-2)e^{\pm(n-1/2)\eta}}{2n-1}\right]\times(n+1)n\cdot C_{n+1}^{-1/2}(\cos\xi), \tag{A24}$$

where the sign $\pm$ is taken as positive for $\eta>0$ and negative for $\eta<0$.

By substituting boundary conditions expressed in Eqs. (A7), (A9), (A11), (A12), and (A14) into Eqs. (A19), (A21), and (A22), we obtain five linear algebra equations with seven variables to be determined. After reduction of some lengthy linear algebra, five of these constants are given as follows:

$$D_n = \frac{\Xi_1+\Xi_2}{\Delta}, \tag{A25}$$

$$A_n = \frac{\mu_2}{\mu_3}D_n, \tag{A26}$$

$$F_n = \frac{\Xi_3-\Xi_4}{\Delta}, \tag{A27}$$

$$E_n = \frac{[(2n-1)B_n+\dot{U}_1]e^{-(n-1/2)\eta_{23}} + [(2n+3)C_n-\dot{U}_2]e^{-(n+3/2)\eta_{23}} + 2\frac{\mu_2}{\mu_3}D_n + \left(n+\frac{3}{2}\right)F_n}{\frac{1}{2}-n}, \tag{A28}$$

$$G_n = D_n\left\{\left(\frac{n}{2}-\frac{1}{4}\right)\sinh\left[\left(n-\frac{1}{2}\right)(\eta_{12}-\eta_{23})\right] - \left(\frac{n}{2}+\frac{3}{4}\right)\sinh\left[\left(n+\frac{3}{2}\right)(\eta_{12}-\eta_{23})\right]\right\} + \left(\frac{n}{2}-\frac{1}{4}\right)E_n\cosh\left[\left(n-\frac{1}{2}\right)(\eta_{12}-\eta_{23})\right] + \left(\frac{n}{2}+\frac{3}{4}\right)F_n\cosh\left[\left(n+\frac{3}{2}\right)(\eta_{12}-\eta_{23})\right] + \frac{\dot{V}}{4}[e^{-(n-1/2)\eta_{12}} - e^{-(n+3/2)\eta_{12}}], \tag{A29}$$

where

$$\dot{V} = \frac{\sqrt{2}}{2}Vc^2(n+1)n, \tag{A30}$$

$$\dot{U}_1 = \sqrt{2}(n+1)nc^2\times\left[W+\frac{U}{2}+\frac{2}{3}c^2R_0^{-2}(n-1)(n-2)(W+U)\right], \tag{A31}$$

$$\dot{U}_2 = \sqrt{2}(n+1)nc^2\times\left[W+\frac{U}{2}+\frac{2}{3}c^2R_0^{-2}(n+3)(n+2)(W+U)\right], \tag{A32}$$

$$\Xi_1 = \{[(2n-1)B_n+\dot{U}_1]e^{-(n-1/2)\eta_{23}} + [(2n+3)C_n-\dot{U}_2]e^{-(n+3/2)\eta_{23}}\}\times\left\{\cosh[(2n+1)(\eta_{12}-\eta_{23})] - \cosh[2(\eta_{12}-\eta_{23})] + \frac{\mu_1}{\mu_2}\sinh[(2n+1)(\eta_{12}-\eta_{23})]\right\}, \tag{A33}$$

$$\Xi_2 = \frac{\dot{V}}{2}e^{-(n-1/2)\eta_{12}}\left(\left[1-\frac{(2n-1)e^{-2\eta_{12}}}{2n+3}\right]\cdot\left\{\frac{\mu_1}{\mu_2}\left(n+\frac{3}{2}\right)\cosh\left[\left(n+\frac{3}{2}\right)(\eta_{12}-\eta_{23})\right]-\frac{\mu_1}{\mu_2}\left(n+\frac{3}{2}\right)\cosh\left[\left(n-\frac{1}{2}\right)(\eta_{12}-\eta_{23})\right]\right.\right.$$
$$\left.+2\sinh\left[\left(n+\frac{3}{2}\right)(\eta_{12}-\eta_{23})\right]\right\}+\left[\frac{\mu_1}{\mu_2}-\left(\frac{\mu_1}{\mu_2}-\frac{4}{2n+3}\right)e^{-2\eta_{12}}\right]\times\left\{\left(n-\frac{1}{2}\right)\sinh\left[\left(n+\frac{3}{2}\right)(\eta_{12}-\eta_{23})\right]\right.$$
$$\left.\left.-\left(n+\frac{3}{2}\right)\sinh\left[\left(n-\frac{1}{2}\right)(\eta_{12}-\eta_{23})\right]\right\}\right), \tag{A34}$$

$$\Xi_3 = \{[(2n-1)B_n+\dot{U}_1]e^{-(n-1/2)\eta_{23}}+[(2n+3)C_n-\dot{U}_2]e^{-(n+3/2)\eta_{23}}\}$$
$$\times\left\{\frac{\mu_1}{\mu_2}\cosh[(2n+1)(\eta_{12}-\eta_{23})]-\frac{\mu_1}{\mu_2}\left(n+\frac{1}{2}\right)\cosh[2(\eta_{12}-\eta_{23})]+\sinh[(2n+1)(\eta_{12}-\eta_{23})]\right.$$
$$\left.-\sinh[2(\eta_{12}-\eta_{23})]+\frac{\mu_1}{\mu_2}\left(n-\frac{1}{2}\right)\right\}, \tag{A35}$$

$$\Xi_4 = \frac{\dot{V}}{2}e^{-(n-1/2)\eta_{12}}\left(\left[1-\frac{(2n-1)e^{-2\eta_{12}}}{2n+3}\right]\cdot\left\{\frac{\mu_1}{\mu_2}\left(n-\frac{1}{2}\right)\sinh\left[\left(n-\frac{1}{2}\right)(\eta_{12}-\eta_{23})\right]-\frac{\mu_1}{\mu_2}\left(n+\frac{3}{2}\right)\sinh\left[\left(n+\frac{3}{2}\right)(\eta_{12}-\eta_{23})\right]\right.\right.$$
$$\left.-2\cosh\left[\left(n+\frac{3}{2}\right)(\eta_{12}-\eta_{23})\right]-2\frac{\mu_1}{\mu_3}\cosh\left[\left(n-\frac{1}{2}\right)(\eta_{12}-\eta_{23})\right]\right\}+\left[\frac{\mu_1}{\mu_2}-\left(\frac{\mu_1}{\mu_2}-\frac{4}{2n+3}\right)e^{-2\eta_{12}}\right]$$
$$\left.\cdot\left\{\left(n-\frac{1}{2}\right)\cosh\left[\left(n-\frac{1}{2}\right)(\eta_{12}-\eta_{23})\right]-\left(n-\frac{1}{2}\right)\cosh\left[\left(n+\frac{3}{2}\right)(\eta_{12}-\eta_{23})\right]-2\frac{\mu_2}{\mu_3}\sinh\left[\left(n-\frac{1}{2}\right)(\eta_{12}-\eta_{23})\right]\right\}\right), \tag{A36}$$

$$\Delta = \left[\frac{2\mu_2}{\mu_3}+\frac{\mu_1}{2\mu_2}(2n+1)^2\right]\cosh[2(\eta_{12}-\eta_{23})]$$
$$-2\left(\frac{\mu_1}{\mu_2}+\frac{\mu_2}{\mu_3}\right)\cosh[(2n+1)(\eta_{12}-\eta_{23})]+(2n+1)$$
$$\times\left(1+\frac{\mu_1}{\mu_3}\right)\sinh[2(\eta_{12}-\eta_{23})]-2\left(1+\frac{\mu_1}{\mu_3}\right)$$
$$\times\sinh[(2n+1)(\eta_{12}-\eta_{23})]-\frac{\mu_1}{\mu_2}(2n-1)\left(n+\frac{3}{2}\right). \tag{A37}$$

B_n and C_n are to be determined in Appendix C by the no-slip boundary condition.

APPENDIX B: CYLINDRICAL COORDINATE SYSTEM

We select the cylindrical coordinate system (R,z) whose origin lies on the center of the outer sphere of the compound drop. Coordinate transformation is written as

$$R = c\frac{\sin\xi}{\cosh\eta-\cos\xi},$$
$$z = z^* - \frac{c}{\tanh\eta_{23}} = c\frac{\sinh\eta}{\cosh\eta-\cos\xi}-\frac{c}{\tanh\eta_{23}}. \tag{B1}$$

General solution for axisymmetric Stokes flow of phase 3 in cylindrical coordinate system is taken as the following separate variable form of stream function:[11]

$$\Psi(R,z) = \int_0^\infty [RK_1(aR)f_1(a)+R^2K_0(aR)F_1(a)$$
$$+RI_1(aR)g_1(a)+R^2I_0(aR)G_1(a)]\cos(az)da$$
$$+\int_0^\infty [RK_1(aR)f_2(a)+R^2K_0(aR)F_2(a)$$
$$+RI_1(aR)g_2(a)+RI_0(aR)G_2(a)]\sin(az)da$$
$$+c_1R^4+c_2R^4z+c_3R^2+c_4R^2z+c_5R^2z^2$$
$$+c_6R^2z^3+c_7z+c_8z^2+c_9z^3, \tag{B2}$$

where K_0 and K_1 are modified Bessel functions of the second kind while I_0 and I_1 are modified Bessel functions of the first kind. The subscripts of the Bessel functions represent their order. f_1, F_1, g_1, G_1, f_2, F_2, g_2, and G_2 are arbitrary derivable functions, c_1-c_9 are integration constants. To satisfy boundary condition (viii) described in Sec. II, Eq. (B2) is reduced to be

$$\Psi(R,z) = \int_0^\infty [RK_1(aR)f_1(a)+R^2K_0(aR)F_1(a)$$
$$+RI_1(aR)g_1(a)+R^2I_0(aR)G_1(a)]\cos(az)da$$
$$+\int_0^\infty [RK_1(aR)f_2(a)+R^2K_0(aR)F_2(a)$$
$$+RI_1(aR)g_2(a)+RI_0(aR)G_2(a)]\sin(az)da$$
$$+\frac{(2W+U)R^2}{2}-\frac{(W+U)R^4}{2R_0^2}. \tag{B3}$$

The no-slip boundary condition at $R=R_0$ for any real value of z leads to

$$\int_0^\infty [R_0K_1(aR_0)f_1(a) + R_0^2K_0(aR_0)F_1(a) + R_0I_1(aR_0)g_1(a) + R_0^2I_0(aR_0)G_1(a)]\cos(az)da + [R_0K_1(aR_0)f_2(a) + R_0^2K_0(aR_0)F_2(a) + R_0I_1(aR_0)g_2(a) + R_0^2I_0(aR_0)G_2(a)]\sin(az)da = 0. \tag{B4}$$

Substituting z by an arbitrary nonzero value and its opposite number into Eq. (B4), either of the two integral parts in Eq. (B4) is zero for any z. Thus, the following two expressions exist:

$$\int_0^\infty [R_0K_1(aR_0)f_1(a) + R_0^2K_0(aR_0)F_1(a) + R_0I_1(aR_0)g_1(a) + R_0^2I_0(aR_0)G_1(a)]da = 0, \tag{B5}$$

$$\int_0^\infty [R_0K_1(aR_0)f_2(a) + R_0^2K_0(aR_0)F_2(a) + R_0I_1(aR_0)g_2(a) + R_0^2I_0(aR_0)G_2(a)]da = 0. \tag{B6}$$

We write the following expressions based on Eqs. (B5) and (B6):

$$g_1(a) = \left(-\frac{2}{a}S_2 - S_4\right)\cdot f_1(a) - R_0^2S_2F_1(a),$$
$$G_1(a) = S_2f_1(a) + S_4F_1(a), \tag{B7}$$

$$g_2(a) = \left(-\frac{2}{a}S_2 - S_4\right)\cdot f_2(a) - R_0^2S_2F_2(a),$$
$$G_2(a) = S_2f_2(a) + S_4F_2(a), \tag{B8}$$

where S_2 and S_4 are expressed as

$$S_2 = \frac{1}{aR_0^2}\cdot\frac{1}{[I_1(aR_0)]^2 - I_0(aR_0)\cdot I_2(aR_0)}, \tag{B9}$$

$$S_4 = \frac{I_1(aR_0)\cdot K_1(aR_0) + I_2(aR_0)\cdot K_0(aR_0)}{[I_1(aR_0)]^2 - I_0(ab)\cdot I_2(aR_0)}. \tag{B10}$$

Following Haberman and Sayre,[11] we expand f_1, F_1, g_1, G_1, f_2, F_2, g_2, and G_2 in the form of Taylor series as

$$f_1(a) = \sum_{n=0}^{\infty} a_n\cdot a^{2n+1}, \quad F_1(a) = \sum_{n=0}^{\infty} b_n\cdot a^{2n},$$
$$f_2(a) = \sum_{n=0}^{\infty} c_n\cdot a^{2n+2}, \quad F_2(a) = \sum_{n=0}^{\infty} d_n\cdot a^{2n+1}. \tag{B11}$$

In order to guarantee nonsingularity of the stream function expressed in Eq. (B3), some terms of the exponential series are omitted in Eq. (B11). The reason will be given later in this section.

Then, substituting

$$I_m(x) = \sum_{k=0}^{\infty}\frac{1}{k!\Gamma(m+k+1)}\cdot\left(\frac{x}{2}\right)^{m+2k} \tag{B12}$$

into the following two-variable functions:

$$\phi_1(R,z) = \int_0^\infty [RI_1(aR)g_1(a) + R^2I_0(aR)G_1(a)+]\times\cos(az)da, \tag{B13}$$

$$\phi_2(R,z) = \int_0^\infty [RI_1(aR)g_2(a) + RI_0(aR)G_2(a)]\sin(az)da, \tag{B14}$$

we have the Taylor expansion at the origin point (0,0) as

$$\phi_1(R,z) = \sum_{L=1}^{\infty}\left[\frac{\int_0^\infty g_1(a)a^{2L-1}da}{2^{2L-1}L!(L-1)!} + \frac{\int_0^\infty G_1(a)a^{2L-2}da}{2^{2L-2}(L-1)!(L-1)!}\right]\cdot R^{2L}\cdot\sum_{m=0}^{\infty}(-1)^m\frac{z^{2m}}{(2m)!}, \tag{B15}$$

$$\phi_2(R,z) = \sum_{L=1}^{\infty}\left[\frac{\int_0^\infty g_2(a)a^{2L-1}da}{2^{2L-1}L!(L-1)!} + \frac{\int_0^\infty G_2(a)a^{2L-2}da}{2^{2L-2}(L-1)!(L-1)!}\right]\cdot R^{2L}\cdot\sum_{m=0}^{\infty}(-1)^m\frac{z^{2m+1}}{(2m+1)!}. \tag{B16}$$

It should be noted that the series in Eqs. (B15) and (B16) are not uniformly convergent. The terms of the series must be arranged in a specific order to guarantee convergence. It is obvious that under spherical coordinate system, series terms $r^nC_n^{-1/2}(\cos\theta)$ of the general solution of the stream function $\Psi(r,\theta)$ are convergent. We find that the sum of terms including $R^{2L}z^{2m}(2L+2m=n)$ in Eqs. (B15) and (B16) corresponds exactly to the series term $r^nC_n^{-1/2}(\cos\theta)$. Therefore, the convergence problem is solved by organizing the sum of Eqs. (B15) and (B16) in this order: first, we sum all terms like $R^{2L}z^{2m}$ where $2L+m$ is a constant value n; second, we do the sum for n from 1 to ∞. Besides, substituting Eqs. (B7), (B8), and (B11) into Eqs. (B15) and (B16), $\phi_1(R,z)$ and $\phi_2(R,z)$ are finally expressed as

$$\phi_1(R,z) = \sum_{N=1}^{\infty}\sum_{k=0}^{N-1}\left[a_k\sum_{L=1}^{N}\frac{\left(2-\frac{2}{L}\right)S_{2,2N+2k-1} - \frac{1}{L}S_{4,2N+k+1}}{R_0^{2N+2k}2^{2L-1}(L-1)!(L-1)!} + b_k\sum_{L=1}^{N}\frac{2S_{4,2N+2k-1} - \frac{1}{L}S_{2,2N+2k-1}}{R_0^{2N+2k-2}2^{2L-1}(L-1)!(L-1)!}\right]\times R^{2L}\sum_{m=0}^{N-L}(-1)^m\frac{z^{2m}}{(2m)!}, \tag{B17}$$

$$\phi_2(R,z)=\sum_{N=1}^{\infty}\sum_{k=0}^{N-1}\left[c_k\sum_{L=1}^{N}\frac{\left(2-\frac{2}{L}\right)S_{2,2N+2k+1}-\frac{1}{L}S_{4,2N+2k+3}}{R_0^{2n+2k+2}2^{2L-1}(L-1)!(L-1)!}+d_k\sum_{L=1}^{N}\frac{2S_{4,2N+2k+1}-\frac{1}{L}S_{2,2N+2k+1}}{R_0^{2N+2k}2^{2L-1}(L-1)!(L-1)!}\right]\times R^{2L}\sum_{m=0}^{N-L}(-1)^m\frac{z^{2m+1}}{(2m+1)!},\tag{B18}$$

where

$$S_{2,n}=\begin{cases}R_0^2\int_0^{\infty}aS_2(aR_0)^{n-1}d(aR_0), & (n>1),\\ 0, & (n=1),\end{cases}\tag{B19}$$

$$S_{4,n}=\begin{cases}\int_0^{\infty}S_4(aR_0)^{n-1}d(aR_0), & (n>1),\\ \int_0^{\infty}\frac{I_1k_1-I_2K_0-\frac{1}{2}}{I_1^2-I_0I_2}d(aR_0), & (n>1).\end{cases}\tag{B20}$$

The integral constant $S_{2,n}$ and $S_{4,n}$ can be evaluated numerically to any precision.

Now we express $\phi_3(R,z)$ and $\phi_4(R,z)$ as

$$\begin{aligned}\phi_3(R,z)&=\int_0^{\infty}[RK_1(aR)f_1(a)+R^2K_0(aR)F_1(a)]\cos(az)da\\&=\int_0^{\infty}\left[\sum_{n=0}^{\infty}a_nRK_1(aR)a^{2n+1}+\sum_{n=0}^{\infty}b_nR^2K_0(aR)a^{2n}\right]\cos(az)da,\end{aligned}\tag{B21}$$

$$\begin{aligned}\phi_4(R,z)&=\int_0^{\infty}[RK_1(aR)f_2(a)+R^2K_0(aR)F_2(a)]\sin(az)da\\&=\int_0^{\infty}\left[\sum_{n=0}^{\infty}c_nRK_2(aR)a^{2n+2}+\sum_{n=0}^{\infty}d_nR^2K_0(aR)a^{2n+1}\right]\sin(az)da.\end{aligned}\tag{B22}$$

Therefore,

$$\Psi(R,z)=\phi_1(R,z)+\phi_2(R,z)+\phi_3(R,z)+\phi_4(R,z)+\frac{(2W+U)R^2}{2}-\frac{(W+U)R^4}{2}.\tag{B23}$$

By successive differentiation of the two following identities with respect to z (Ref. 17):

$$\int_0^{\infty}R^2K_0(aR)\cos(az)da=\frac{\pi}{2}\frac{R^2}{(R^2+z^2)^{1/2}},\tag{B24}$$

$$\int_0^{\infty}aRK_1(aR)\cos(az)da=\frac{\pi}{2}\frac{R^2}{(R^2+z^2)^{3/2}},\tag{B25}$$

we obtain

$$\int_0^{\infty}a^{2j}R^2K_0(aR)\cos(az)da=\frac{\pi}{2}\sum_{i=0}^{j}\frac{c_{2j,i}R^{2(i+1)}}{(R^2+z^2)^{j+i+1/2}},\tag{B26}$$

$$\int_0^{\infty}a^{2j+1}R^2K_0(aR)\sin(az)da=\frac{\pi}{2}\sum_{i=0}^{j}\frac{c_{2j+1,i}R^{2(i+1)}z}{(R^2+z^2)^{j+i+3/2}},\tag{B27}$$

$$\int_0^{\infty}a^{2j+1}RK_1(aR)\cos(az)da=\frac{\pi}{2}\sum_{i=0}^{j}\frac{d_{2j+1,i}R^{2(i+1)}}{(R^2+z^2)^{j+i+3/2}},\tag{B28}$$

$$\int_0^{\infty}a^{2j+2}RK_1(aR)\sin(az)da=\frac{\pi}{2}\sum_{i=0}^{j}\frac{d_{2j+2,i}R^{2(i+1)}z}{(R^2+z^2)^{j+i+5/2}},\tag{B29}$$

where $c_{j,i}$ and $d_{j,i}$ are constants to be determined, and the subscripts ε and j are integers starting from zero. The recurrence formulas about $c_{j,i}$ and $d_{j,i}$ are

$$\begin{aligned}c_{2j+1,i}&=(2j+2i+1)c_{2j,i},\\c_{2j+2,i}&=(2j+2i+1)c_{2j+1,i-1}-2(j+i+1)c_{2j+1,i},\\c_{2j+2,j+1}&=(4j+3)c_{2j+1,j},\\c_{2j+2,0}&=-2(j+1)c_{2j+1,0}\quad(i=1,2,3,\ldots,j),\end{aligned}\tag{B30}$$

$$d_{2j+2,i} = (2j+2i+3)d_{2j+1,i},$$

$$d_{2j+3,i} = (2j+2i+3)d_{2j+2,i-1} - 2(j+i+2)c_{2j+2,i},$$

$$d_{2j+3,j+1} = (4j+5)d_{2j+2,j}, \tag{B31}$$

$$d_{2j+3,0} = -2(j+2)d_{2j+2,0} \quad (i = 1,2,3,\ldots,j).$$

The integrals $\int_0^\infty a^{2j+1}R^2K_0(aR)\cos(az)da$, $\int_0^\infty a^{2j}R^2K_0(aR)\sin(az)da$, $\int_0^\infty a^{2j}RK_1(aR)\cos(az)da$, and $\int_0^\infty a^{2j+1}RK_1(aR)\sin(az)da$ lead to infinite axial velocity at the axis of the circular tube, if they serve as parts of the stream function. Therefore, they must be omitted from the solution, yielding the expressions in Eq. (B11).

APPENDIX C: TRANSFORMATION BETWEEN CYLINDRICAL AND BIPOLAR COORDINATE SYSTEMS

Since $\phi_1(R,z)$ and $\phi_2(R,z)$ are in the form of sum of $R^{2L}z^m$ for $L>0$, $m\geq 0$ and $z=z^*-c/\tanh\eta_{23}$, where L and m are integers, we first convert the term $R^{2L}z^{*m}$ to the form of $(\cosh\eta-\cos\xi)^{-3/2}\cdot\Sigma_{n=1}^{\infty}\Theta_n(\eta)\cdot C_{n+1}^{-1/2}(\cos\xi)$ under bipolar coordinate system. The definition and properties of Gegenbauer polynomials are[18]

$$\frac{1}{(1-2xt+t^2)^\lambda} = \sum_{n=0}^{\infty} C_n^\lambda(x)t^n, \tag{C1}$$

$$\text{for } \lambda > -1/2: \begin{cases} \displaystyle\int_{-1}^{1}(1-x^2)^{\lambda-1/2}C_n^\lambda(x)C_m^\lambda(x)dx = 0 & \text{for } m\neq n, \\ \displaystyle\int_{-1}^{1}(1-x^2)^{\lambda-1/2}C_n^\lambda(x)C_n^\lambda(x)dx = \frac{2^{1-2\lambda}\pi\cdot\Gamma(n+2\lambda)}{(n+\lambda)\Gamma^2(\lambda)\Gamma(n+1)} & \text{for } m=n, \end{cases} \tag{C2}$$

$$\text{for } \lambda=-1/2 \quad \text{and} \quad m,n>1: \begin{cases} \displaystyle\int_{-1}^{1}\frac{C_n^{-1/2}(x)C_m^{-1/2}(x)dx}{1-x^2} = 0 & \text{for } m\neq n, \\ \displaystyle\int_{-1}^{1}\frac{C_n^{-1/2}(x)C_m^{-1/2}(x)dx}{1-x^2} = \frac{2}{(2n-1)n(n-1)} & \text{for } m=n, \end{cases} \tag{C3}$$

$$\frac{d}{dx}C_n^\lambda(x) = 2\lambda C_n^{\lambda+1}(x), \tag{C4}$$

$$(n+\lambda)C_n^\lambda(x) = \lambda C_n^{\lambda+1}(x), \tag{C5}$$

$$nC_n^\lambda(x) = 2(n+\lambda-1)xC_{n-1}^\lambda(x) - (n+2\lambda-2)C_{n-2}^\lambda(x). \tag{C6}$$

Due to orthogonality of Gegenbauer polynomials given in Eqs. (C2) and (C3), $\Theta_n(\eta)$ $(n>0)$ is written as

$$\Theta_n(\eta) = \frac{n(n+1)(2n+1)}{2}\int_{-1}^{1} c^{2L+m}\frac{(1-x^2)^{L-1}C_{n+1}^{-1/2}(x)}{(\cosh\eta-x)^{2L+m-1/2}}dx, \tag{C7}$$

where $x=\cos\xi$. Through integration by parts and substitution of Eq. (C6) into Eq. (C7), we obtain

$$\Theta_n(\eta) = \frac{n(n+1)(2n+1)}{2}\times\int_{-1}^{1}\frac{c^{2L+m}(1-x^2)^{L-2}}{(\cosh\eta-x)^{2L+m-3/2}}\cdot\frac{(n+2L-1)(n+2)C_{n+2}^{-1/2}(x)-(n-2L+2)(n-1)C_n^{-1/2}(x)}{\left(2L+m-\frac{5}{2}\right)\cdot(2n+1)}dx. \tag{C8}$$

We perform the above process $L-1$ times for Eq. (C7), yielding

$$\Theta_n(\eta) = \frac{n(n+1)(2n+1)}{2}\int_{-1}^{1}\frac{1}{\Pi_{i=1}^{L-1}2L+m-i-\frac{3}{2}}\cdot\frac{c^{2L+m}}{(\cosh\eta-x)^{L+m-1/2}}\cdot\sum_{i=1}^{L}\alpha_{n,L,i}C_{n-L+2i}^{-1/2}dx, \tag{C9}$$

where $\alpha_{n,L,i}$ is a constant to be determined. Using integration by parts and with the help of Eq. (C4), we convert Eq. (C9) to

$$\Theta_n(\eta) = \frac{n(n+1)(2n+1)}{2}\int_{-1}^{1}\frac{1}{\Pi_{i=1}^{L}2L+m-i-\frac{3}{2}}\cdot\frac{c^{2L+m}\sinh^m\eta}{(\cosh\eta-x)^{L+m-3/2}}\cdot\sum_{i=1}^{L}\alpha_{n,L,i}P_{n-L+2i-1}dx, \tag{C10}$$

where $P_n(x)$ is the Gegenbauer polynomials of degree 1/2, i.e., Legendre polynomials of the first kind. The factor $(\cosh\eta - x)^{-(L+m-3/2)}$ in Eq. (C10) can be expanded through the generation function of Gegenbauer polynomials of Eq. (C1) as

$$\frac{1}{(\cosh\eta - x)^{L+m-3/2}} = \sum_{j=0}^{\infty} 2^{L+m-3/2} e^{-(j+L+m-3/2)\eta} C_j^{L+m-3/2}(x) \quad (\eta > 0). \tag{C11}$$

By recursive substitution of Eq. (C5), we obtain

$$C_n^{L+m-3/2}(x) = \beta_{n,L+m,1} C_n^{1/2}(x) + \beta_{n,L+m,2} C_{n-2}^{1/2}(x) + \beta_{n,L+m,4} C_{n-4}^{1/2}(x) + \cdots \quad \text{for } L,m > 1, \tag{C12}$$

where $C_n^{1/2}(x)$ is $P_n(x)$, and $\beta_{n,L+m,1}$, $\beta_{n,L+m,2}\cdots$ are constants to be determined. Due to orthogonality of $P_n(x)$,

$$\int_{-1}^{1} P_n(x) P_m(x) dx = \begin{cases} \dfrac{2}{2n+1} & (m=n), \\ 0 & (m \neq n), \end{cases} \tag{C13}$$

it is obvious that $\Theta_n(\eta)$ only consists of terms including different integer exponents of $e^{-\eta/2}$. Since $\phi_1(R,z)$ and $\phi_2(R,z)$ are stream functions under cylindrical coordinate system, they must satisfy the general solution form when converted under bipolar coordinate system. Therefore, we only retain the terms of $e^{-(n-1/2)\eta}$ and $e^{-(n+3/2)\eta}$ in $\Theta_n(\eta)$, while other terms of $\Theta_n(\eta)$ must offset each other when summed together. We denote the retained terms in $\Theta_n(\eta)$ as $\Theta_n^*(\eta)$, which can be derived from Eqs. (C10)–(C13) as

$$\Theta_n^*(\eta) = \frac{2^{L-3/2} c^{2L+m} n(n+1)(2n+1)}{q_{L,m}} \cdot \left\{ \frac{\alpha_{n,L,1}\beta_{n-L+1,L+m,1}}{2n-2L+3} e^{-(n-1/2)\eta} + \left[\frac{\alpha_{n,L,2}\beta_{n-L+3,L+m,1}}{2n-2L+7} + \frac{\alpha_{n,L,1}(\beta_{n-L+3,L+m,2} - m\beta_{n-L+1,L+m,1})}{2n-2L+3} \right] e^{-(n+3/2)\eta} \right\}, \tag{C14}$$

where

$$q_{L,m} = \prod_{i=1}^{L} 2L + m - i - \frac{3}{2}, \tag{C15}$$

$$\alpha_{n,L,1} = (-1)^{L-1} \prod_{i=1}^{L-1} \frac{(n-2L+i+1)(n-i)}{2n-2i+3}, \tag{C16}$$

$$\alpha_{n,L,2} = (-1)^{L} \sum_{i=0}^{L-2} \left[\prod_{j=1}^{i} \frac{(n-2L+j+1)(n-j)}{2n-2j+3} \right] \times \frac{(n+2L-3i-1)(n-i+2)}{2n-2i+1} \times \left[\prod_{j=i}^{L-3} \frac{(n-2L+j+5)(n-j)}{2n-2j+3} \right], \tag{C17}$$

$$\beta_{n,L+m,1} = \begin{cases} \displaystyle\prod_{i=1}^{L+m-2} \frac{n+L+m-i-\frac{3}{2}}{L+m-i-\frac{3}{2}} & (L+m>1), \\ -\dfrac{1}{2n-1} & (L=1,\ m=0), \\ 0 & (n<0), \end{cases} \tag{C18}$$

$$\beta_{n,L+m,2} = \begin{cases} \displaystyle\sum_{i=0}^{L+m-3} \left[\prod_{j=1}^{i} \frac{n+L+m-j-\frac{3}{2}}{L+m-j-\frac{3}{2}} \right] \times \frac{n+L+m-i-\frac{9}{2}}{L+m-i-\frac{5}{2}} \times \left[\prod_{j=i+2}^{L+m-2} \frac{n+L+m-j-\frac{7}{2}}{L+m-j-\frac{3}{2}} \right], & (L+m>1), \\ \dfrac{1}{2n-1}, & (L=1,\ m=0), \\ 0, & (n<0). \end{cases} \tag{C19}$$

Substituting Eq. (C14) into Eqs. (B17) and (B18), we finally obtain the expressions of ϕ_1 and ϕ_2 under bipolar coordinate system as

$$\phi_1(R,z)=\sum_{N=1}^{\infty}\sum_{k=0}^{N-1}\left[a_k\sum_{L=1}^{N}\frac{\left(2-\frac{2}{L}\right)S_{2,2N+2k-1}-\frac{1}{L}S_{4,2N+k+1}}{R_0^{2N+2k}2^{2L-1}(L-1)!(L-1)!}+b_k\sum_{L=1}^{N}\frac{2S_{4,2N+2k-1}-\frac{1}{L}S_{2,2N+2k-1}}{R_0^{2N+2k-2}2^{2L-1}(L-1)!(L-1)!}\right]$$
$$\times\sum_{m=0}^{N-L}\frac{(-1)^m}{(2m)!}(\cosh\eta-\cos\xi)^{-3/2}\sum_{n=1}^{\infty}C_{n+1}^{-1/2}(\cos\xi)\frac{2^{L-3/2}c^{2L+2m}n(n+1)(2n+1)}{q_{L,2m}}$$
$$\times\left\{\frac{\alpha_{n,L,1}\beta_{n-L+1,L+2m,1}}{2n-2L+3}e^{-(n-1/2)\eta}+\left[\frac{\alpha_{n,L,1}(\beta_{n-L+3,L+2m,2}-2m\beta_{n-L+1,L+2m,1})}{2n-2L+3}+\frac{\alpha_{n,L,2}\beta_{n-L+3,L+2m,1}}{2n-2L+7}\right]e^{-(n+3/2)\eta}\right\},\tag{C20}$$

$$\phi_2(R,z)=\sum_{N=1}^{\infty}\sum_{k=0}^{N-1}\left[a_k\sum_{L=1}^{N}\frac{\left(2-\frac{2}{L}\right)S_{2,2N+2k-1}-\frac{1}{L}S_{4,2N+k+1}}{R_0^{2N+2k}2^{2L-1}(L-1)!(L-1)!}+b_k\sum_{L=1}^{N}\frac{2S_{4,2N+2k-1}-\frac{1}{L}S_{2,2N+2k-1}}{R_0^{2N+2k-2}2^{2L-1}(L-1)!(L-1)!}\right]$$
$$\times\sum_{m=0}^{N-L}\frac{(-1)^m}{(2m+1)!}(\cosh\eta-\cos\xi)^{-3/2}\sum_{n=1}^{\infty}C_{n+1}^{-1/2}(\cos\xi)\frac{2^{L-3/2}c^{2L+2m+1}n(n+1)(2n+1)}{q_{L,2m+1}}$$
$$\times\left(\frac{\alpha_{n,L,1}\beta_{n-L+1,L+2m+1,1}}{2n-2L+3}e^{-(n-1/2)\eta}+\left\{\frac{\alpha_{n,L,1}[\beta_{n-L+3,L+2m+1,2}-(2m+1)\beta_{n-L+1,L+2m+1,1}]}{2n-2L+3}\right.\right.$$
$$\left.\left.+\frac{\alpha_{n,L,2}\beta_{n-L+3,L+2m+1,1}}{2n-2L+7}\right\}\right)e^{-(n+3/2)\eta}.\tag{C21}$$

Now we deal with the integrals related to the second kind of modified Bessel functions in $\phi_3(R,z)$ and $\phi_4(R,z)$. First, like what we do previously in this section, we convert the term $R^{2(i+1)}/(R^2+z^2)^{j+i+1/2}$ in Eqs. (B26) and (B28) to the form like $(\cosh\eta-\cos\xi)^{-3/2}\cdot\Sigma_{n=1}^{\infty}\Theta_{n,1}(\eta)\cdot C_{n+1}^{-1/2}(\cos\xi)$ under bipolar coordinate system. Using the relationship between the two coordinate systems, we get

$$R^2+z^2=\frac{c^2\sin^2\xi}{(\cosh\eta-\cos\xi)^2}+\frac{c^2\sinh^2\eta}{(\cosh\eta-\cos\xi)^2}-\frac{2c^2\sinh\eta\cosh\eta_{23}}{\sinh\eta_{23}(\cosh\eta-\cos\xi)}+\frac{c^2\cosh^2\eta_{23}}{\sinh^2\eta_{23}}=\frac{c^2[\cosh(\eta-2\eta_{23})-\cos\xi]}{\sinh^2\eta_{23}(\cosh\eta-\cos\xi)}.\tag{C22}$$

Therefore, $\Theta_{n,1}(\eta)$ is expressed as

$$\Theta_{n,1}(\eta)=\frac{n(n+1)(2n+1)}{2}\frac{\sinh^{2j+2i+1}\eta_{23}}{c^{2j-1}}\int_{-1}^{1}\frac{(1-x^2)^{2i}(\cosh\eta-x)^{j-i}}{[\cosh(\eta-2\eta_{23})-x]^{i+j+1/2}}C_{n+1}^{-1/2}(x)dx.\tag{C23}$$

Applying a little algebra transformation $\cosh\eta-x=\cosh(\eta-2\eta_{23})-x+2\sinh(\eta-\eta_{23})\sinh\eta_{23}$ to Eq. (C23), we obtain

$$\Theta_{n,1}(\eta)=\frac{n(n+1)(2n+1)}{2}\frac{\sinh^{2j+2i+1}\eta_{23}}{c^{2j-1}}\times\int_{-1}^{1}\sum_{k=0}^{j-i}\frac{(1-x^2)^{2i}[2\sinh(\eta-\eta_{23})\sinh\eta_{23}]^k C_{n+1}^{-1/2}(x)}{[\cosh(\eta-2\eta_{23})-x]^{2i+k+1/2}}\binom{j-i}{k}dx.\tag{C24}$$

It is easy to observe from Eq. (C24) that $\Theta_{n,1}(\eta)$ only consists of terms with different integer exponents of $e^{(n-1/2)(\eta-2\eta_{23})}$ and $e^{(n+3/2)(\eta-2\eta_{23})}$, which is similar to what appears in the transformation for $R^{2L}z^{*m}$. Thus, we likewise retain only the terms of integer exponents of $e^{(n-1/2)(\eta-2\eta_{23})}$ and $e^{(n+3/2)(\eta-2\eta_{23})}$ in $\Theta_{n,1}(\eta)$ to form $\Theta_{n,1}^{*}(\eta)$. We derived $\Theta_{n,1}^{*}(\eta)$ from Eqs. (C11)–(C13) and (C24) as

$$\Theta_{n,1}^{*}(\eta)=\frac{2^{i-1/2}(n+1)(2n+1)\sinh^{2j+2i+1}\eta_{23}}{c^{2j-1}q_{i+1,k}}\sum_{k=0}^{j-i}\binom{j-i}{k}(e^{-2\eta_{23}}-1)^k\left\{\frac{\alpha_{n,i+1,1}\beta_{n-i,i+k+1,1}}{2n-2i+1}\times e^{(n-1/2)(\eta-2\eta_{23})}\right.$$
$$\left.+\left[\frac{\alpha_{n,i+1,1}(\beta_{n-i+2,i+k+1,2}-ke^{2\eta_{23}}\beta_{n-i,i+k+1,1})}{2n-2i+1}+\frac{\alpha_{n,i+1,2}\beta_{n-i+2,i+k+1,1}}{2n-2i+5}\right]\times e^{(n+3/2)(\eta-2\eta_{23})}\right\}.\tag{C25}$$

Second, after transforming the term $R^{2(i+1)}z/(R^2+z^2)^{j+i+3/2}$ in Eqs. (B27) and (B29) into the form like $(\cosh\eta-\cos\xi)^{-3/2}\cdot\Sigma_{n=1}^{\infty}\Theta_{n,2}(\eta)\cdot C_{n+1}^{-1/2}(\cos\xi)$, we obtain

$$\Theta_{n,2}(\eta)=\frac{n(n+1)(2n+1)\sinh^{2j+2i+3}\ \eta_{23}}{2c^{2j}}\int_{-1}^{1}\left\{\sum_{k=0}^{j-i}\frac{(1-x^2)^{2i}[2\ \sinh(\eta-\eta_{23})\sinh\ \eta_{23}]^k\sinh\ \eta}{[\cosh(\eta-2\eta_{23})-x]^{2i+k+3/2}}\binom{j-i}{k}\right.$$
$$\left.-\sum_{k=0}^{j-i+1}\frac{(1-x^2)^{2i}[2\ \sinh(\eta-\eta_{23})\sinh\ \eta_{23}]^k}{[\cosh(\eta-2\eta_{23})-x]^{2i+k+1/2}\tanh\ \eta_{23}}\binom{j-i+1}{k}\right\}C_{n+1}^{-1/2}(x)dx. \tag{C26}$$

In the same way, $\Theta_{n,2}^{*}(\eta)$ is written as

$$\Theta_{n,2}^{*}(\eta)=\frac{2^{i-1/2}(n+1)(2n+1)\sinh^{2j+2i+3}\ \eta_{23}}{c^{2j}}\left\{\sum_{k=0}^{j-i}\binom{j-i}{k}\frac{-(e^{-2\eta_{23}}-1)^k}{e^{2\eta_{23}}q_{i+1,k+1}}\left[\frac{\alpha_{n,i+1,1}\beta_{n-i,i+k+2,1}}{(2n-2i+1)}\times e^{(n-1/2)(\eta-2\eta_{23})}\right.\right.$$
$$\left.+\left(\frac{\alpha_{n,i+1,1}[\beta_{n-i+2,i+k+2,2}-(ke^{2\eta_{23}}+e^{4\eta_{23}})\beta_{n-i,i+k+2,1}]}{2n-2i+1}+\frac{\alpha_{n,i+1,2}\beta_{n-i+2,i+k+2,1}}{2n-2i+5}\right)\times e^{(n+3/2)(\eta-2\eta_{23})}\right]$$
$$-\sum_{k=0}^{j-i+1}\binom{j-i+1}{k}\frac{(e^{-2\eta_{23}}-1)^k}{q_{i+1,k}\tanh\ \eta_{23}}\left[\frac{\alpha_{n,i+1,1}\beta_{n-i,i+k+1,1}}{(2n-2i+1)}e^{(n-1/2)(\eta-2\eta_{23})}\right.$$
$$\left.\left.+\left(\frac{\alpha_{n,i+1,1}(\beta_{n-i+2,i+k+1,2}-ke^{2\eta_{23}}\beta_{n-i,i+k+1,1})}{2n-2i+1}+\frac{\alpha_{n,i+1,2}\beta_{n-i+2,i+k+1,1}}{2n-2i+5}\right)e^{(n+3/2)(\eta-2\eta_{23})}\right]\right\}. \tag{C27}$$

By the aid of Eqs. (C26) and (C27), we may easily write the coefficients of the terms $e^{(n-1/2)(\eta-2\eta_{23})}$ and $e^{(n+3/2)(\eta-2\eta_{23})}$ for stream function $\Psi(R,z)$ in Eq. (B3), which is expanded under bipolar coordinate system. Excluding the part for Poiseuille flow $(W+U/2)R^2-(W+U)R^4/2$, the coefficient of $e^{(n-1/2)(\eta-2\eta_{23})}$ is

$$\sum_{j=0}^{\infty}b_j\sum_{i=0}^{j}c_{2j,i}\frac{2^{i-1/2}(n+1)(2n+1)\sinh^{2j+2i+1}\ \eta_{23}}{c^{2j-1}q_{i+1,k}}\sum_{k=0}^{j-i}\binom{j-i}{k}(e^{-2\eta_{23}}-1)^k\frac{\alpha_{n,i+1,1}\beta_{n-i,i+k+1,1}}{2n-2i+1}$$
$$-\sum_{j=0}^{\infty}d_j\sum_{i=0}^{j}c_{2j+1,i}\frac{2^{i-1/2}(n+1)(2n+1)\sinh^{2j+2i+3}\ \eta_{23}}{c^{2j}}$$
$$\times\left[\sum_{k=0}^{j-i}\binom{j-i}{k}\frac{(e^{-2\eta_{23}}-1)^k}{e^{2\eta_{23}}q_{i+1,k+1}}\frac{\alpha_{n,i+1,1}\beta_{n-i,i+k+2,1}}{2n-2i+1}+\sum_{k=0}^{j-i+1}\binom{j-i+1}{k}\frac{(e^{-2\eta_{23}}-1)^k}{q_{i+1,k}\tanh\ \eta_{23}}\frac{\alpha_{n,i+1,1}\beta_{n-i,i+k+1,1}}{2n-2i+1}\right]$$
$$+\sum_{j=0}^{\infty}a_j\sum_{i=0}^{j}d_{2j+1,i}\frac{2^{i-1/2}(n+1)(2n+1)\sinh^{2j+2i+3}\ \eta_{23}}{c^{2j+1}q_{i+1,k}}\sum_{k=0}^{j-i}\binom{j-i+1}{k}(e^{-2\eta_{23}}-1)^k\frac{\alpha_{n,i+1,1}\beta_{n-i,i+k+1,1}}{2n-2i+1}$$
$$-\sum_{j=0}^{\infty}c_j\sum_{i=0}^{j}d_{2j+2,i}\frac{2^{i-1/2}(n+1)(2n+1)\sinh^{2j+2i+5}\ \eta_{23}}{c^{2j+2}}\left[\sum_{k=0}^{j-i}\binom{j-i+1}{k}\frac{(e^{-2\eta_{23}}-1)^k}{e^{2\eta_{23}}q_{i+1,k+1}}\frac{\alpha_{n,i+1,1}\beta_{n-i,i+k+2,1}}{2n-2i+1}\right.$$
$$\left.+\sum_{k=0}^{j-i+1}\binom{j-i+2}{k}\frac{(e^{-2\eta_{23}}-1)^k}{q_{i+1,k}\tanh\ \eta_{23}}\frac{\alpha_{n,i+1,1}\beta_{n-i,i+k+1,1}}{2n-2i+1}\right]. \tag{C28}$$

For $e^{(n+3/2)(\eta-2\eta_{23})}$, the coefficient is

$$\sum_{j=0}^{\infty}b_j\sum_{i=0}^{j}c_{2j,i}\frac{2^{i-1/2}(n+1)(2n+1)\sinh^{2j+2i+1}\ \eta_{23}}{c^{2j-1}q_{i+1,k}}\sum_{k=0}^{j-i}\binom{j-i}{k}(e^{-2\eta_{23}}-1)^k$$
$$\times\left[\frac{\alpha_{n,i+1,2}\beta_{n-i+2,i+k+1,1}}{2n-2i+5}+\frac{\alpha_{n,i+1,1}(\beta_{n-i+2,i+k+1,2}-ke^{2\eta_{23}}\beta_{n-i,i+k+1,1})}{2n-2i+1}\right]$$
$$-\sum_{j=0}^{\infty}d_j\sum_{i=0}^{j}c_{2j+1,i}\frac{2^{i-1/2}(n+1)(2n+1)\sinh^{2j+2i+3}\ \eta_{23}}{c^{2j}}\left\{\sum_{k=0}^{j-i}\binom{j-i}{k}\frac{(e^{-2\eta_{23}}-1)^k}{e^{2\eta_{23}}q_{i+1,k+1}}\left[\frac{\alpha_{n,i+1,2}\beta_{n-i+2,i+k+2,1}}{2n-2i+5}\right.\right.$$
$$\left.+\frac{\alpha_{n,i+1,1}[\beta_{n-i+2,i+k+2,2}-(ke^{2\eta_{23}}+e^{4\eta_{23}})\beta_{n-i,i+k+2,1}]}{2n-2i+1}\right]+\sum_{k=0}^{j-i+1}\binom{j-i+1}{k}\frac{(e^{-2\eta_{23}}-1)^k}{q_{i+1,k}\tanh\ \eta_{23}}$$
$$\left.\times\left[\frac{\alpha_{n,i+1,2}\beta_{n-i+2,i+k+1,1}}{2n-2i+5}+\frac{\alpha_{n,i+1,1}(\beta_{n-i+2,i+k+1,2}-ke^{2\eta_{23}}\beta_{n-i,i+k+1,1})}{2n-2i+1}\right]\right\}$$

$$+\sum_{j=0}^{\infty} a_j \sum_{i=0}^{j} d_{2j+1,i} \frac{2^{i-1/2}(n+1)(2n+1)\sinh^{2j+2i+3}\eta_{23}}{c^{2j+1} q_{i+1,k}} \sum_{k=0}^{j-i} \binom{j-i}{k} (e^{-2\eta_{23}}-1)^k$$
$$\times \left[\frac{\alpha_{n,i+1,2}\beta_{n-i+2,i+k+1,1}}{2n-2i+5} + \frac{\alpha_{n,i+1,1}(\beta_{n-i+2,i+k+1,2} - ke^{2\eta_{23}}\beta_{n-i,i+k+1,1})}{2n-2i+1} \right]$$
$$-\sum_{j=0}^{\infty} c_j \sum_{i=0}^{j} d_{2j+2,i} \frac{2^{i-1/2}(n+1)(2n+1)\sinh^{2j+2i+5}\eta_{23}}{c^{2j+2}} \left\{ \sum_{k=0}^{j-i} \binom{j-i}{k} \frac{(e^{-2\eta_{23}}-1)^k}{e^{2\eta_{23}} q_{i+1,k+1}} \left[\frac{\alpha_{n,i+1,2}\beta_{n-i+2,i+k+2,1}}{2n-2i+5} \right.\right.$$
$$\left.\left. + \frac{\alpha_{n,i+1,1}[\beta_{n-i+2,i+k+2,2} - (ke^{2\eta_{23}} + e^{4\eta_{23}})\beta_{n-i,i+k+2,1}]}{2n-2i+1} \right] + \sum_{k=0}^{j-i+1} \binom{j-i+1}{k} \frac{(e^{-2\eta_{23}}-1)^k}{q_{i+1,k}\tanh\eta_{23}} \right.$$
$$\times \left[\frac{\alpha_{n,i+1,2}\beta_{n-i+2,i+k+1,1}}{2n-2i+5} + \frac{\alpha_{n,i+1,1}(\beta_{n-i+2,i+k+1,2} - ke^{2\eta_{23}}\beta_{n-i,i+k+1,1})}{2n-2i+1} \right]. \quad \text{(C29)}$$

By combination of Eqs. (B3), (C20), (C21), (C28), and (C29), we completely transform the stream function $\Psi(R,z)$ into the form under bipolar coordinate system. Since $\Psi(R,z)$ and $\Psi^{(3)}(\eta,\xi)$ are equivalent functions under different coordinate systems, each term of the series in $\Psi^{(3)}$ must be exactly equal to that of the expansion form of $\Psi(R,z)$ under bipolar coordinate system. Therefore, by equalizing the coefficients of $e^{-(n-1/2)\eta}$, $e^{-(n+3/2)\eta}$, $e^{(n-1/2)(\eta-2\eta_{23})}$, and $e^{(n+3/2)(\eta-2\eta_{23})}$ between $\Psi^{(3)}(\eta,\xi)$ [expressed by Eq. (A19) for $\eta>0$] and the expansion form of $\Psi(R,z)$ under bipolar coordinate system [Eqs. (B3), (A23), (A24), (C20), (C21), (C28), and (C29)], we obtain a set of infinite algebra linear equations like $A\mathbf{X}=b$ with variables a_j, b_j, c_j, d_j, B_n, and C_n. If we limit N in Eqs. (C20) and (C21) to a finite even number N^*, and j in Eqs. (C28) and (C29) to $N^*/2$, we in fact truncate the stream function $\Psi^{(3)}(\eta,\xi)$, which is equivalent to truncate the stream function under spherical coordinate system (r,θ) with the first N^* terms. Therefore, the number of variables to be determined becomes $4N^*$. Besides, for a specific n, the comparison of the coefficients ($e^{-(n-1/2)\eta}$, $e^{-(n+3/2)\eta}$, $e^{(n-1/2)(\eta-2\eta_{23})}$, and $e^{(n+3/2)(\eta-2\eta_{23})}$) yields four linear equations. Hence, n should be from 1 to N^* to form $4N^*$ linear equations to make the equation set complete. The solution precision can be as high as required by increasing N^*. As a_j, b_j, c_j, and d_j are determined, $\Psi(R,z)$ is determined. Thus, it is easy to deduce B_n^* and C_n^* in Eq. (A20) if the flow field for $\eta<0$ is needed.

[1] K. J. Lissant, *Emulsion and Emulsion Technology* (Marcel Dekker, New York, 1974), Vol. 6.
[2] A. S. Utada, E. Lorenceau, D. R. Link, P. D. Kaplan, H. A. Stone, and D. A. Weitz, "Monodisperse double emulsions generated from a microcapillary device," Science **308**, 537 (2005).
[3] W. Seifriz, "Double reversal of oil emulsions occasioned by the same electrolyte," J. Phys. Chem. **29**, 738 (1925).
[4] L. Y. Chu, A. S. Utada, R. K. Shah, J. W. Kim, and D. A. Weitz, "Controllable monodisperse multiple emulsions," Angew. Chem., Int. Ed. **46**, 8970 (2007).
[5] T. Nisisako, S. Okushima, and T. Torii, "Controlled formulation of monodisperse double emulsions in a multiple-phase microfluidic system," Soft Matter **1**, 23 (2005).
[6] P. Garstecki, H. A. Stone, and G. M. Whitesides, "Mechanism for flow-rate controlled breakup in confined geometries, a route to monodisperse emulsions," Phys. Rev. Lett. **94**, 164501 (2005).
[7] T. G. Mason, S. M. Graves, J. N. Wilking, and M. Y. Lin, "Extreme emulsification, formation and structure of nanoemulsions," Condens. Matter Phys. **9**, 193 (2006).
[8] J. H. Xu, S. W. Li, J. Tan, Y. J. Wang, and G. S. Luo, "Controllable preparation of monodisperse O/W and W/O emulsions in the same microfluidic device," Langmuir **22**, 7943 (2006).
[9] C. Zhou, P. Yue, and J. J. Feng, "Formation of simple and compound drops in microfluidic devices," Phys. Fluids **18**, 092105 (2006).
[10] C. Zhou, P. Yue, and J. J. Feng, "Deformation of a compound drop through a contraction in a pressure-driven pipe flow," Int. J. Multiphase Flow **34**, 102 (2008).
[11] W. L. Haberman and R. M. Sayre, "Motion of rigid and fluid spheres in stationary and moving liquids inside cylindrical tubes," David Taylor Model Basin Report No. 1143, Department of the Navy, US, 1958.
[12] S. S. Sadhal and H. N. Oguz, "Stokes flow past compound multiphase drops, the case of completely engulfed drops bubbles," J. Fluid Mech. **160**, 511 (1985).
[13] H. N. Oguz and S. S. Sadhal, "Growth and collapse of translating compound multiphase drops: Analysis of fluid mechanics and heat transfer," J. Fluid Mech. **179**, 105 (1987).
[14] M. J. Martinez and K. S. Udell, "Axisymmetric creeping motion of drops through circular tubes," J. Fluid Mech. **210**, 565 (1990).
[15] G. B. Jeffery, "On a form of the solution of Laplace's equation suitable for problems relating to two spheres," Proc. R. Soc. London, Ser. A **87**, 109 (1912).
[16] L. Pasol, M. Chaoui, and S. Yahiaoui, "Analytical solutions for a spherical particle near a wall in axisymmetrical polynomial creeping flows," Phys. Fluids **17**, 073602 (2005).
[17] W. Magnus and F. Oberhettinger, *Formulas and Theorems for the Special Functions of Mathematical Physics*, 3rd ed. (Springer-Verlag, New York, 1966).
[18] G. Szegö, *Orthogonal Polynomials*, 4th ed. (American Mathematical Society, Providence, 1975).